Turkish Journal of Earth Sciences (Turkish J. Earth Sci.), **Vol. 15**, 2006, pp. 181-209. *Copyright ©TÜBİTAK*

Geochemical Constraints on the Provenance, Mineral Sorting and Subaerial Weathering of Lower Jurassic and Upper Cretaceous Clastic Rocks of the Eastern Pontides, Yusufeli (Artvin), NE Turkey

ABDURRAHMAN DOKUZ[1] & ERKAN TANYOLU[2]

[1]Karadeniz Technical University, Gümüşhane Engineering Faculty, Department of Geological Engineering, TR–29000 Gümüşhane, Turkey (E-mail: dokuz@ktu.edu.tr)
[2]Fırat University, Department of Geological Engineering, TR–23119 Elazığ, Turkey

Abstract: An integrated petrographic and geochemical study of the shales and sandstones of Early Jurassic and Late Cretaceous age in the Yusufeli area (Turkey) was carried out to obtain more information on their provenance, sedimentological history and tectonic setting, as well as to evaluate the influence of weathering, hydraulic sorting and recycling processes upon source-rock signature. Depending on their matrix and mineralogical content, the Lower Jurassic sandstones are identified as arkosic arenite and wacke, while the Upper Cretaceous sandstones are defined as lithic arenite and wacke.

Elemental ratios such as La/Sc, Cr/Ni, Co/Th, Th/Sc and Cr/Th indicate a mafic source for the majority of each of the sandstone sequences. However, in several samples, high Th/Sc and low Cr/Th ratios suggest a contribution from a felsic source. Using element-ratio diagrams, all of the samples plot along a curve consistent with a two-component mixing model, consisting of a dominant mafic and a subordinate felsic source. The relatively low Cr/Ni ratios provide no support for significant amounts of ultramafic lithologies in the source area. The lower trace-element contents of the studied sandstones in relation to post-Archean Australian shales (PAAS), which are representative of the composition of the upper continental crust, indicate that recycling processes in their source areas were probably less intense than those of the PAAS. The more LREE-depleted patterns of the shales relative to sandstones likely do not reflect changes in source-area composition but, rather, variations in mineral sorting, chemical weathering and/or sediment recycling.

Chemical index of alteration (CIA) indices observed in the Lower Jurassic and Upper Cretaceous sediments (average of 53 & 46, respectively) suggest that their source area underwent moderate degrees of chemical weathering processes. However, an upward increase in the values of the CIA indices in the Lower Jurassic profiles may indicate that the source area gradually underwent more intense chemical weathering, possibly due to climatic and/or tectonic variations. On the other hand, an upward decrease in the CIA indices of the Upper Cretaceous profiles generally demonstrate that the sediments were derived from a relatively less-weathered source terrain, reflecting an increased erosion rate likely due to increasing tectonic activity.

The compositional immaturity of the analysed sandstone samples is typical of subduction-related environments, and their SiO_2/Al_2O_3 and K_2O/Na_2O ratios and Co, Sc, Th and Zr contents reflect their oceanic and continental-arc settings.

Key Words: shale and sandstone, geochemistry, provenance, hydraulic sorting, alteration, Yusufeli-Artvin, northeastern Turkey

Doğu Pontidler'deki Erken Jura ve Geç Kretase Yaşlı Kırıntılı Kayaçların Kaynak Alanı, Mineral Boylanması ve Yüzeysel Ayrışması Üzerine Jeokimyasal Sınırlamalar, Yusufeli (Artvin), KD Türkiye

Özet: Yusufeli (Artvin) yöresindeki Erken Jura ve Geç Kretase yaşlı şeyl ve kumtaşları; kaynak alanları, sedimantolojik gelişimleri ve tektonik ortamları hakkında daha fazla bilgi edinmek, ayrışma, hidrolik boylanma ve tortul-döngü olaylarının kaynak alan karakteristikleri üzerindeki etkisini değerlendirmek amacı ile petrografik ve jeokimyasal açıdan incelenmiştir. Hamur (matriks) ve mineralojik içeriklerine göre, Erken Jura yaşlı kumtaşları arkozik arenit ve vake, Geç Kretase kumtaşları ise litik arenit ve vake olarak tanımlanmışlardır.

La/Sc, Cr/Ni, Co/Th, Th/Sc ve Cr/Th gibi element oranları her iki istif için de mafik bir kaynak alana işaret etmektedir. Bununla birlikte, bir çok örnekteki yüksek Th/Sc ve düşük Cr/Th oranları da felsik bir kaynağın katkısını öngörmektedir. Örnekler, kullanılan oransal diyagramlarda, mafik ve felsik kaynakların katkısı ile oluşan iki bileşenli bir karışım eğrisi boyunca dağılmaktadırlar. Göreli olarak düşük Cr/Ni oranları, kaynak alanda ultramafik litolojilerin olmadığına işaret etmektedir. Kumtaşlarının, üst kıtasal kabuk bileşimini temsil ettiği düşünülen post-Arkeen Avusturalya şeyllerine (PAAS) göre daha az bollukta iz element içerikleri, kaynak alanlarındaki tortul-döngü olaylarının olasılıkla daha az yoğunlukta olduğuna işaret etmektedir. Şeylerin kumtaşlarına göre daha fazla tüketilmiş hafif nadir toprak element dağılımları da, kaynak alandaki kayaçların bileşimlerindeki değişimden ziyade mineral boylanması, kimyasal ayrışma ve/veya tortul-döngüdeki değişimleri yansıtmaktadır.

Alt Jura ve Üst Kretase tortullarında gözlenen kimyasal ayrışma indeksi (chemical index of alteration = CIA) (sırası ile ortalama 53 ve 46) kaynak alanlarının orta derecede kimyasal ayrışma olaylarına uğradığını öngörmektedir. Bununla birlikte, CIA indeksinin Alt Jura istiflerinde yukarıya doğru artması; kaynak alanın, olasılıkla iklim ve tektonik değişimler nedeniyle, giderek daha fazla kimyasal ayrışmaya uğradığını gösterebilir. Diğer taraftan, Üst Kretase istiflerinde CIA indeksinin yukarı doğru genel bir azalımı; tortulların göreli olarak daha az ayrışan bir kaynaktan kaynaklandığını göstermekte ve olasılıkla da artan tektonik etkinlik nedeni ile artan erozyon oranını yansıtmaktadır.

Analiz edilen kumtaşlarının bileşimsel olarak olgunlaşmamış olması yitimle ilişkili ortamların tipik özelliğidir. SiO_2/Al_2O_3, K_2O/Na_2O oranları ve Co, Sc, Th ve Zr içerikleri okyanussal ada yayı ve kıtasal yay ortamlarını göstermektedir.

Anahtar Sözcükler: şeyl ve kumtaşı, modal analiz, jeokimya, kaynak alan, hidrolik boylanma, kimyasal ayrışma indeksi, Yusufeli-Artvin, Kuzeydoğu Türkiye

Introduction

Clastic sedimentary rocks are indicators of past environments, giving clues to their compositions and even to their geodynamic settings by means of their compositions. The provenance and geodynamic development of sandstone successions can be classified by a variety of methods, including petrographic analysis, whole-rock and mineral chemistry. Above all, clastic sediments can supply information on continental and oceanic source regions that have been eroded or metamorphosed through subsequent tectonic processes (Nesbitt & Young 1982; McLennan 1989; McLennan *et al.* 1993; Cullers 1994; Condie *et al.* 1995). In terrigenous rocks, some detrial minerals are characteristic of certain source rocks and source regions. Thus, often only the detrial components of clastic rocks reveal clues to source areas that have disappeared. The present study uses petrographic and geochemical methods on Lower Jurassic and Upper Cretaceous sandstones and shales from the Yusufeli (Artvin) area to decipher the influence of source-rock characteristics, chemical weathering during transport and sedimentation, and post-depositional diagenetic reactions, all affecting the chemical record of their compositions and, consequently, evidence concerning their parental affinities (Nesbitt 1979; Cullers *et al.* 1979, 1987; Banfield & Eggelton 1989; McLennan 1989; McLennan *et al.* 1993; Condie *et al.* 1995).

In this regard, it seems obvious that the Lower Jurassic clastic succession has been derived from pre-Jurassic basement that is currently represented by mainly medium- to high-grade metamorphic rocks of Carboniferous age (e.g., the Artvin-Yusufeli area metamorphic rocks, Pulur Massif: Dokuz 2000; Topuz *et al.* 2004; Topuz & Altherr 2004) and cross-cutting high-K granitoids of Permian age (e.g., the Gümüşhane and Köse granitoids: Yılmaz 1972; Bergougnan 1987). However, while the rock fragments derived metamorphic rocks and granitoids are nearly absent, plagioclase and volcanic lithic fragments form the main components in these rocks. The main question here is whence these volcanic fragments have been derived. Were they derived from the Late Palaeozoic basement where their exposures do not include such volcanic rocks (Yılmaz 1972; Bergougnan 1987; Okay 1996; Dokuz 2000; Topuz *et al.* 2004; Yılmaz & Yılmaz 2004; Erdoğan & Güngör 2004; Koralay *et al.* 2004; Gerdjikov 2005), or syn-sedimentarily from Lower Jurassic volcanic activity? Do they correspond to volcanic clastics derived from the associated extrusive equivalents (Bozkuş 1990) of Permian granitoid rocks (which are presently unexposed or nonexistent)? Similar questions are valid for the second, or Upper Cretaceous regressive, clastic succession. For instance, we have an imperfect understanding concerning whether the source area was the same or different from those materials deposited in the Early Jurassic, and whether certain parts of the pre-Jurassic basement were maintained or were not in their 'source position' until the end of Mesozoic. In the light of

the lack of geochemical data from the Mesozoic clastic rocks, the elemental abundance data and source-area interpretations that we present will help to elucidate the paleogeographical conditions of this area. In a more general context, this study offers a chance to understand in detail the effects of various sedimentary processes on the geochemical signature of sedimentary rocks. Although analyses of fine-clastic sediments, such as shales, are usually emphasized in geochemical provenance studies, this sample set also allows direct comparison between sandstones and shales. Assuming that sandstones and shales of the same age are cogenetic, comparison of the chemical compositions of the two different lithologies allows an evaluation of the control of the hydraulic sorting on elemental distributions.

Regional Geological Framework

The Pontides, one of the major tectonic units of Turkey, is a paleo-island arc ranging from Mid-Eocene to Late Palaeozoic in age (Ketin 1966; Akın 1978; Şengör & Yılmaz 1981; Akıncı 1984; Bozkurt & Mittwede 2001). Its eastern part is conventionally divided into northern and southern zones (Akın 1978; Gedikoğlu *et al.* 1979; Okay & Şahintürk 1997; Bektaş *et al.* 1999) that differ from each other in terms of rock associations. In the northern zone, comprising the axial part of the arc, Cretaceous to Eocene basic and acidic volcanic rocks with Kuroko-type ore deposits and coeval granitoids predominate (Arslan *et al.* 1997; Şen *et al.* 1998; Karslı *et al.* 2004; Aslan 2005) (Figure 1). In the southern zone, the Mesozoic section is represented predominantly by sedimentary units that unconformably overlie the Hercynian metamorphic and granitic basesement (Yılmaz 1972; Çoğulu 1975; Gedikoğlu *et al.* 1979; Keskin *et al.* 1989; Okay 1996; Dokuz 2000; Topuz *et al.* 2004; Topuz & Altherr 2004; Yılmaz & Yılmaz 2004). It is generally agreed that the Mesozoic basin opened from the Permian until the Dogger as a back arc-basin south of the Pontian arc and is a consequence of a southward-dipping oceanic lithosphere (Şengör *et al.* 1980; Şengör & Yılmaz 1981; Bektaş *et al.* 1984; Tüysüz 1990; Chatalov 1991; Ustaömer & Robertson 1993; Yılmaz *et al.* 1997; Okay & Şahintürk 1997; Floyd *et al.* 2003; Okay & Göncüoğlu 2004; Pickett & Robertson 2004; Dean 2005). The Hamurkesen formation constitutes the lowermost part of the Mesozoic units and comprises pillow basalts, basaltic to andesitic lithic tuffs, sandstones and shales, which locally contain 'ammonitico rosso' horizons. This succession has been interpreted as a product of a magmatic arc undergoing rifting (Şengör *et al.* 1980; Şengör & Yılmaz 1981; Yılmaz *et al.* 1997; Okay & Şahintürk 1997; Floyd *et al.* 2003). Upper Jurassic to Lower Cretaceous platform-type carbonates concordantly overlie Middle Jurassic fine-grained clastic rocks and are ascribed to the quiescent period that followed rapid tectonic subsidence. The major change in tectonic style – from extensional to compressional – began in the Albian–Cenomanian (Tüysüz *et al.* 1995; Okay & Şahintürk 1997; Yılmaz *et al.* 1997); this records a regressive turbiditic succession in the southern zone, and volcanic to volcaniclastic rocks – associated with their intrusive equivalents – in the northern zone throughout the eastern Pontides. It is suggested that the absence of Palaeocene to Early Eocene lithologies, in general, may be explained by the Mesozoic basin being raised up to sea level at the end of the Upper Cretaceous. From the Palaeocene to Early Eocene, the continental margin was telescoped into a series of stacked north-vergent thrust slices, as a consequence of major shortening along the southern zone. Timing the initiation of subduction and continental collision is contentious. Some authors suggest that subduction began during the Jurassic or even earlier (Adamia *et al.* 1977), while others postulate that its onset was initiated during the Cenomanian–Turonian (Şengör & Yılmaz 1981; Tüysüz et al 1995; Okay & Şahintürk 1997). Most workers relate the Eocene volcanism to the northward subduction of the Tethyan ocean floor, and have considered that the collision occurred during the Oligocene (Tokel 1977; Akın 1978; Robinson *et al.* 1995), while Okay & Şahintürk (1997) maintained a Late Palaeocene–Early Eocene age for continental collision between the Pontides and the Anatolide-Tauride Platform on the basis of the absence of deformation in the Eocene rocks.

Stratigraphy

In the study area, the Lower Jurassic Hamurkesen formation unconformably overlies the metamorphic basement (Figure 2) and is of variable thickness. The maximun thickness of the formation, about 964 m, was measured near the village of İşhan. Although an Early–Middle Jurassic age has been assigned to the formation based on its stratigraphic location in the study area, it is not necessarily reliable. However, in some early

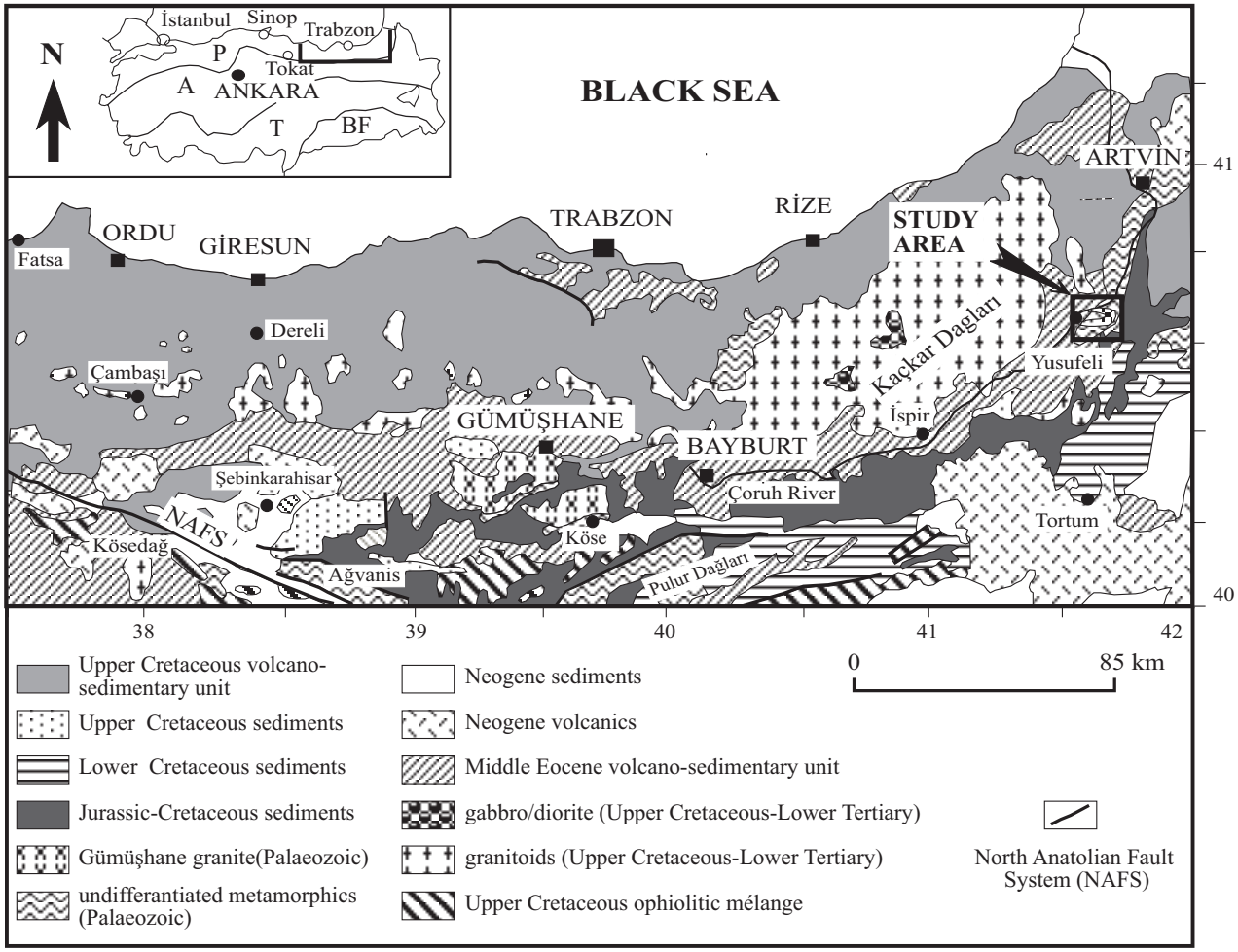

Figure 1. Simplified geological map of the east of the eastern Pontides (modified after the Geological Map of Turkey, scale 1/500,000, MTA 1961) and the location of the mapped area. Inset shows the tectonic units of Turkey with the location of eastern Pontides. **P**– Pontides, **A**– Anatolides, **T**– Taurides and **BF**– Border Folds (from Ketin 1966).

papers (Alp 1972; Yılmaz 1972; Özer 1984), an early Pliensbachian to Toarcian age was reported for the lower boundary, largely based on ammonites from the 'ammonitico rosso' horizons. As for the upper boundary, the presence of a Kimmeridgian microfossil assemblage (*Protopenerolis striata* Weynschenk, *Trocholina alpina* Leupold, *Koskinobullina socialis* Cherci & Schroeder, *Nantilaculina oolitica* Mohler) in the micritic limestone at the base of the overlying carbonates (Berdiga formation) indicate a pre-Kimmeridgian age for the top of the formation (Kemal Erdoğan, personal communication 2000). Dokuz (2000) described the formation as consisting of two stratigraphic units: (i) a lower unit of pillowed and massive basalt and basaltic andesite intercalated with some thin-bedded silts and shales, and (ii) an upper unit of shallow-water sedimentary rocks with some interbedded basic volcanic rocks. The lava flows of the lower unit are massive or pillowed, with the pillows typically 0.5–1 m in diameter; the pillows possess chilled margins and calcite-, chlorite-, zeolite- and quartz-filled vesicles. Locally, massive basalt grades into pillow basalt, possibly indicating – in part – that the massive variety represents extrusive lava flows. Intrusive rocks (dolerite stocks) are scarce in the Hamurkesen formation and include narrow (< 2 m), cross-cutting doleritic dykes. Coal-bearing, thin-bedded green shale is the first component of the upper unit that overlies the basalts. Upward, the succession grades into a sandstone-shale alternation about 500 m thick and includes intercalated basic tuffs, agglomerates and breccias, from several

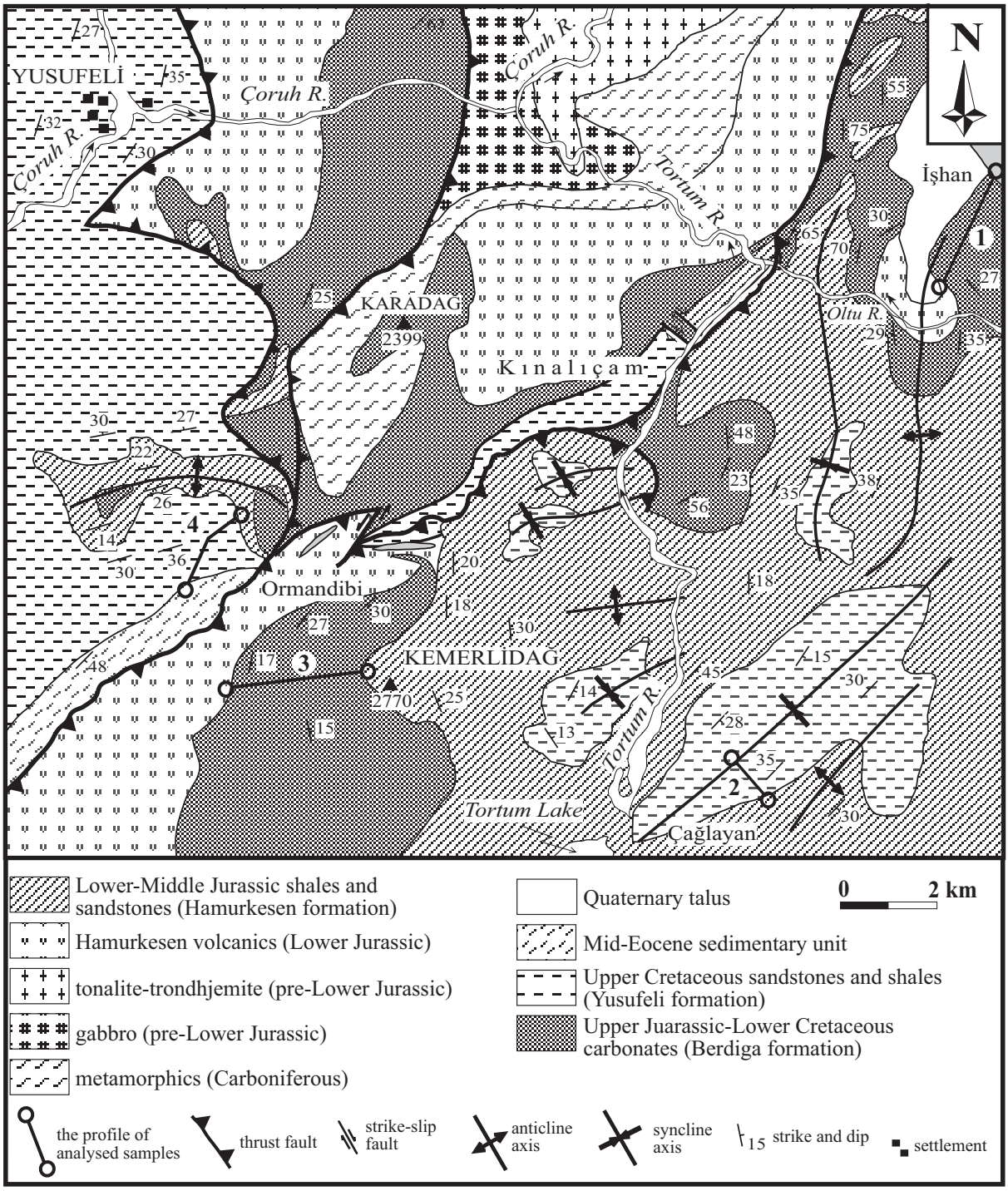

Figure 2. Detailed geological map of the Yusufeli (Artvin) area, including profiles of the analysed samples (modified from Dokuz 2000).

metres up to 66 m in thickness. The top of the unit is represented by about 450 m of shales. The Hamurkesen formation and its equivalents have been interpreted by many workers as the basin-fill deposits of an extensional rift (Şengör *et al.* 1980; Şengör & Yılmaz 1981; Bektaş *et al.* 1984; Chatalov 1991; Ustaömer & Robertson

1993; Yılmaz *et al.* 1997; Okay & Şahintürk 1997; Floyd *et al.* 2003). Crustal stretching has been attributed to the ascent of a mantle plume that gave rise to the extrusion of the underlying Hamurkesen volcanic rocks.

On the basis of the determined important taxa and genera (i.e., *Hedbergella trocoidea* Gandolfi, *Hedbergella delrioensis* Carsey, *Globigerina hoterivica* Subbotina, *Meandrospira favrei* Charrolias, Brönniman & Zaninetti, *Tintinopsella carpathica* Murgeanu & Filipescu, *Alveosepta jaccardi* Schrodt, *Protopeneroplis* cf. *trochangulata* Septfontaine, *Tubiphytes morronensis* Crescenti, *Conicospirillina basiliensis* Mohler, *Pseudosyclammina lituus* Yokoyama) (Kemal Erdoğan, personal communication 2000), the age of the platform-type carbonates (Berdiga formation) can be constrained as Kimmeridgian–Barremian. The Yusufeli formation is represented by arc-derived turbidites of regressive character and was deposited over the carbonate rocks during the Aptian–Campanian time interval (*Globotruncana bulloides* Vogler, *Globotruncana linneiana* d' Orbigny, *Rosita fornicata* Plummer, *Pithonella ovalis* Kaufmann, *Stomiosphaera sphaerica* Kaufmann, *Marssonella oxcona* Reus, *Lagenidae marginotruncana coronata* Bolli, *Marginotruncana pseudolinneiana* Pessagno, *Rotalipora ticinensis* Gaundolfi, *Rotalipora reichelli* Mornod, *Globigerinelloides ferreolensis* Moullade, *Hedbergela trocoidea* Gaundolfi) (Kemal Erdoğan, personal communication 2000). The unit consists entirely of sedimentary rocks to the south of the area, whereas intermediate and acidic volcanic rocks are incorporated into the unit with increasing order to the north. It comprises red-clastic lithologies (sandstone, siltstone, shale, micritic limestone, and chert) at four stratigraphic horizons: one at the bottom, two in the middle and another one at the top of the sequence. The rest of the unit consists of grey to green sandstones and siltstones, and subordinate shales. Some basaltic and acidic volcanic levels (up to 4 m thick) are also present. Bed thickness and grain size gradually increase upward within the unit. North of the study area, the turbidites pass vertically and laterally into massive volcanic rocks intermediate to felsic in nature. The bulk of the volcanic rocks are of island-arc calc-alkaline nature (Dokuz 2000). Palaeocene sediments are absent in the area. The Eocene overlies the Late Cretaceous Yusufeli formation along an angular unconformity and commences with a basal conglomerate bounded by a red matrix. The nummulite-bearing sandstones and limestones, which overlie the conglomerate, have yielded a Lutetian age for the initiation of sediment deposition.

Sampling and Analytical Methods

The present study is based on modal mineralogical and geochemical analyses of shales and sandstones from four complete profiles (İşhan, Kemerlidağ, Ormandibi and Çağlayan) through the Lower Jurassic and Upper Cretaceous sequence (Figure 3). A total of 36 medium- to fine-grained samples (11 from the profiles of the Lower Jurassic Hamurkesen formation and 25 from the profiles of the Upper Cretaceous Yusufeli formation) were point-counted for detrital modal analysis with a semi-automatic Swift Point Counter (Table 1; geochemically non-analysed samples are not shown). Depending on groundmass content, at least 350–500 grains per sample were counted. To minimize the effects of grain-size variations, rock fragments were counted using the Gazzi-Dickinson method (Dickinson & Suczek 1979). All components below 0.063 mm apparent diameter (silt and clay fraction) were counted as matrix, as were cement crystals regardless of size. Each thin section was stained for K-feldspar. After a thin section was etched in concentrated hydrofluoric acid for 5 s, it was plunged into a solution prepared by mixing 100 ml of water with 60 ml Na-hegzanitrocobaltat to obtain canary yellow for K-feldspar. According to the Gazzi-Dickinson method, we were able to distinguish the following framework constituents: quartz (Q), including monocrystalline and polycrystalline varieties; feldspar (F), comprising plagioclase (P) and K-feldspar (AF); lithic fragments (L), comprising basaltic-dacitic volcanic and sedimentary clasts; matrix (M); cement (C); hornblende (hb); biotite (bi); and heavy minerals (HM). Heavy minerals include opaque grains (magnetite, ilmenite) and chlorite. For the nomenclature of shale samples, the chemical classification diagram of Creaser *et al.* (1997) was used.

Bulk-rock chemical compositions of 36 samples were determined partly by inductively coupled plasma-mass spectrometry (ICP-MC) at the commercial Acme Analytical Laboratories Ltd. in Vancouver, Canada. In the ICP-MS analyses, a 0.2 g aliquot is weighed into a graphite crucible and mixed with 1.5 g of LiBO2 flux. The crucibles are placed in an oven and heated to 1050 ºC for 15 minutes. The molten sample is dissolved in 5% HNO3

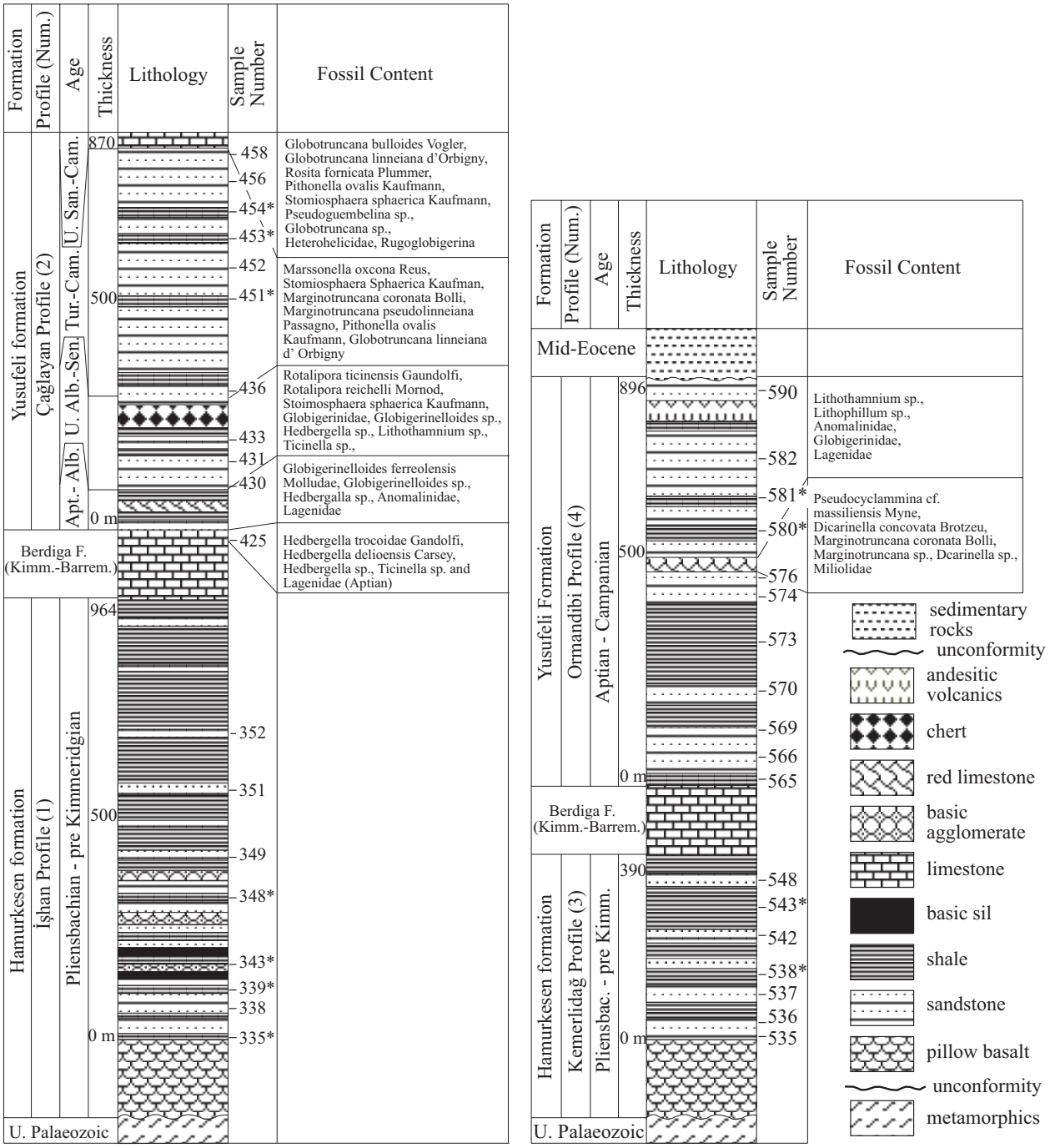

Figure 3. Simplified stratigraphic logs of the Lower Jurassic and Upper Cretaceous units with sample localities of modal-mineralogically and geochemically analysed shales (marked with asteriks) and sandstones. Localities of some sandstones, which were merely analysed in terms of modal mineralogical content, are not shown.

(ACS-grade nitric acid diluted in demineralized water). Calibration standards and reagent blanks are added to the sample sequence. Sample solutions are aspirated into an ICP emission spectrograph (Jarrel Ash Atom Comb 975) for determining major oxides and certain trace elements (Ba, Nb, Ni, Sr, Sc, Y & Zr), while the sample solutions

Table 1. Mineralogical and chemical compositions of analysed samples and the PAAS (Taylor & McLennan 1985). Major elements are reported in weight percent and trace elements in ppm. Weight percent oxides are recalculated to 100% on a volatile-free basis.

	Lower Jurassic samples																Upper Cretaceous s.		
	İşhan profile								Kemerlidağ profile								Çağlayan profile		
	shales					sandstones			sandstones					shales			shales		
	349	335	339	343	348	338	349	351	352	535	536	537	542	548	538	543	PAAS	451	453	454
Q						10.4	3.0	2.2	2.0	10.2	5.4	1.8	16.6	2.0						
Pl						29	30.6	33.2	32.2	63.2	53.4	52.2	66.8	52.2						
AF						19.2	2.8	4.4	2.2	0.0	0.6	0.6	0.0	0.0						
L						35	29.8	27.4	34	10.2	7.6	18.6	7.2	8.8						
HM						3.4	1.4	0.4	1.6	2.6	0.8	5.2	1.0	1.8						
M						2.6	0.0	0.0	0.0	13.2	30.2	16.2	7.4	0.0						
C						0.0	32.4	32.4	26.2	0.0	0.0	4.4	0.0	35.2						
hb,bi						0.4	0.0	0.0	1.8	0.6	1.6	1.0	1.0	0.0						
%																				
SiO_2	80.63	78.13	80.44	67.25		75.20	55.12	52.43	56.08	63.78	72.47	60.08	68.14	60.59	60.20	60.96	62.4	48.63	62.63	64.13
TiO_2	0.39	0.55	0.21	0.67		0.47	0.73	0.93	0.65	0.90	0.55	0.63	0.51	0.61	0.83	0.62	0.99	0.52	0.37	0.32
Al_2O_3	7.15	9.35	9.05	14.92		12.03	18.11	17.13	17.24	15.64	13.46	17.70	17.31	17.57	18.73	18.48	18.78	18.30	17.19	17.80
Fe_2O_3	5.40	3.76	4.33	6.31		4.32	6.75	5.36	5.64	8.85	5.05	6.58	3.53	4.78	7.82	8.28	7.18	4.81	4.17	4.49
MnO	0.03	0.06	0.09	0.08		0.09	0.32	0.29	0.30	0.09	0.04	0.11	0.02	0.08	0.11	0.09	-	0.24	0.08	0.06
MgO	1.50	1.40	1.22	3.06		1.34	1.50	1.55	1.92	3.43	2.04	2.26	1.29	0.82	3.19	2.47	2.19	2.11	1.99	2.37
CaO	0.63	1.37	1.35	3.97		2.80	13.40	18.10	12.92	0.92	1.84	5.18	5.19	9.06	0.28	5.12	1.29	19.41	7.68	1.97
Na_2O	0.46	0.38	2.93	3.02		1.86	2.58	2.60	3.22	5.95	3.88	6.08	3.63	4.74	6.78	2.97	1.19	4.70	4.74	8.29
K_2O	3.69	4.96	0.33	0.67		1.85	1.45	1.60	1.91	0.21	0.61	1.28	0.27	1.62	1.94	0.82	3.68	1.25	1.09	0.40
P_2O_5	0.11	0.04	0.04	0.06		0.03	0.04	0.01	0.12	0.22	0.06	0.11	0.11	0.14	0.12	0.20	0.16	0.01	0.05	0.16
ppm																				
Rb	152	89	4.0	16		28	19.9	20	27	-	-	-	-	-	22	-	160	12.8	17.7	-
Sr	23	361	109	404		652	389	372	364	366	407	293	144	245	132	198	200	1113	546	554
Cs	3.3	3.5	0.3	0.7		-	0.6	0.7	2.3	-	-	-	-	-	0.3	2.4	15	7.0	4.0	-
Ba	220	442	447	190		470	246	244	201	71	174	168	88	212	489	250	650	240.1	275.8	124
Th	3.5	1	2.8	4.2		8.42	2.5	1.6	1.3	-	-	-	-	-	4.7	9.4	14.6	0.8	2.6	-
U	0.4	0.3	0.7	1.8		0.5	0.7	0.4	0.4	-	-	-	-	-	1.0	1.5	3.1	0.6	1.2	-
Zr	46.5	33.7	95.9	68.7		75	57.2	41.6	48.1	210	110	45	80	55	96.2	131.2	210	31	55	58
Hf	1.2	1	2.8	2.3		3.82	1.8	1.3	1.6	-	-	-	-	-	2.9	4.0	5	0.8	2.1	-
Y	15.7	13.5	32.1	16.3		14	22.6	31.3	32.5	12	11	6.3	5.5	4.7	16.2	15.7	27	10.3	7.3	10
Nb	3	1.8	3.9	5.3		3.4	4.6	2.8	2.3	15	11	10	10	10	7.1	13.7	1.9	1.4	1.7	10
Cr	4.789	27.37	27.37	6.842		27.37	20.5	47.89	41.05	20.53	20.53	34.21	6.842	54.74	34.21	27.37	110	27.37	34.21	61.58
Co	6.5	5.8	25	2.5		-	13.5	10.4	12.9	-	-	-	-	-	17.6	6.8	23	11.1	11.5	-
Ni	11.1	6.7	1.9	7.1		21	10	6.4	8.2	-	-	-	-	-	29	7.4	55	12.4	20.6	-
Cu	65.6	71.2	37.9	33.8		-	25.8	28.7	21.5	-	-	-	-	-	-	33.2	50	11.8	75.4	-
Sc	13	24	11	19		11	13	11	14	14	10	12	10	10	19	11	16	10	10	10
V	123	184	12	133		-	129	145	144	-	-	-	-	-	201	116	150	98	85	-
La	9.1	6.1	10	15		7.6	17.2	26.4	20.1	29.1	-	-	20.9	-	13.4	17.6	38.2	8.4	8.7	-
Ce	17	10.5	21.9	33.5		12.8	31.6	47.4	35.7	51.3	-	-	32.7	-	23.4	31.7	79.6	14.1	16.1	-
Pr	2.17	1.36	2.59	3.67		1.55	3.76	5.19	4.34	6.69	-	-	3.85	-	2.97	3.64	8.83	1.78	2.01	-
Nd	10.2	6.4	11.4	13		6.2	15.2	21.1	17.2	20.84	-	-	11.98	-	13	13.5	33.9	7.7	7.2	-
Sm	2.4	1.7	3.1	3.2		1.69	3.20	4.1	4.1	3.66	-	-	2.13	-	2.7	2.6	5.55	1.5	1.4	-
Eu	0.6	0.57	0.98	0.71		0.81	0.86	0.78	1.01	0.97	-	-	0.97	-	0.76	0.72	1.08	0.61	0.51	-
Gd	2.33	1.97	3.63	2.9		1.75	3.52	4.16	4.36	3.16	-	-	1.82	-	3.08	2.38	4.66	1.68	1.33	-
Tb	0.46	0.35	0.74	0.5		0.5	0.56	0.74	0.72	0.66	-	-	0.42	-	0.48	0.41	0.77	0.29	0.2	-
Dy	2.82	2.56	4.57	2.89		2.44	3.62	3.84	4.68	2.61	-	-	1.54	-	3	2.59	4.68	1.62	1.08	-
Ho	0.55	0.54	0.99	0.59		0.54	0.82	1.03	1.1	0.46	-	-	0.3	-	0.61	0.53	0.99	0.37	0.26	-
Er	1.44	1.43	3.22	1.77		2.02	2.30	2.65	3.13	1.57	-	-	1.0	-	1.74	1.45	2.85	0.96	0.67	-
Tm	0.27	0.2	0.47	0.26		0.33	0.34	0.42	0.49	0.23	-	-	0.14	-	0.3	0.24	0.40	0.15	0.1	-
Yb	1.6	1.38	2.85	1.75		1.76	2.34	2.67	3.36	1.26	-	-	0.81	-	1.93	1.65	2.82	0.94	0.75	-
Lu	0.26	0.19	0.51	0.26		0.29	0.32	0.47	0.51	0.21	-	-	0.13	-	0.33	0.24	0.43	0.16	0.12	-

Table 1. continued

	Upper Cretaceous samples																		
	Çağlayan profile							Ormandibi profile											
	sandstones							sandstones									shales		
	430	431	433	436	452	456	458	565	566	569	570	573	574	576	582	590	580	581	
Q	3.4	2.8	3.2	1.0	3.4	2.6	3.8	0.0	0.0	0.0	0.4	0.4	10	19.2	5.4	9.0			
Pl	33.8	27.8	20	29.4	8.8	34	28.4	24.2	32	30.2	17.8	14	5.2	20.8	28	5.6			
AF	0.0	0.0	0.0	0.4	0.9	0.0	0.0	0.0	0.0	0.0	0.0	0.0	4.4	1.6	0.2	0.0			
L	32.4	39.2	36.6	23.2	82.9	31.8	41.5	56.4	65.2	63.2	66	54.6	60.6	35.2	47.4	79.8			
HM	6.6	3.4	5.8	13.6	0.7	1.2	4.4	5.8	1.2	0.6	9.6	1.4	0.2	0.0	4.6	5.6			
M	0.0	0.0	0.0	0.0	0.0	0.0	20.2	13.6	1.2	5.4	5.8	0.0	0.0	0.0	0.0	0.0			
C	19.2	25.2	32.6	32	3.4	12.8	0.0	0.0	0.0	0.0	0.0	29.2	19.6	23	10.6	0.0			
hb, bi	4.6	1.6	1.8	0.4	0.9	17.6	1.7	0.0	0.4	0.6	0.4	0.4	0.0	0.2	3.8	0.0			
%																			
SiO_2	52.63	51.36	47.98	50.98	57.31	54.72	68.33	63.16	63.29	65.90	60.34	55.02	67.40	71.88	52.28	76.29	62.75	68.91	
TiO_2	0.62	0.67	0.77	0.87	0.61	0.45	0.65	0.59	0.75	0.50	0.74	0.83	0.56	0.20	0.76	0.45	0.57	0.06	
Al_2O_3	16.89	16.20	15.08	16.98	16.64	17.39	15.93	19.15	17.77	17.66	19.19	14.73	13.63	8.21	15.63	15.55	14.73	11.95	
Fe_2O_3	7.01	7.09	8.66	5.49	7.84	5.32	4.01	5.30	5.46	4.12	5.75	3.15	3.62	1.43	8.86	3.98	6.39	4.19	
MnO	0.16	0.17	0.18	0.09	0.13	0.11	0.04	0.05	0.05	0.04	0.06	0.14	0.14	0.07	0.16	0.03	0.16	0.10	
MgO	1.88	1.54	2.19	1.03	3.85	2.96	0.95	2.75	2.20	0.96	1.21	4.45	2.79	0.71	3.87	0.88	1.96	2.13	
CaO	15.31	17.58	19.54	20.07	8.50	13.92	3.39	3.11	1.39	1.60	5.82	17.15	6.15	13.88	13.75	1.63	8.99	8.24	
Na_2O	3.90	3.76	3.86	2.97	3.17	4.15	4.44	4.36	7.91	8.68	5.08	3.76	4.98	1.48	3.73	0.26	3.18	2.84	
K_2O	1.54	1.51	1.62	1.46	1.86	0.84	2.12	1.29	0.99	0.42	1.68	0.63	0.52	2.13	0.87	0.88	1.11	1.17	
P_2O_5	0.06	0.12	0.12	0.06	0.09	0.12	0.15	0.23	0.19	0.12	0.12	0.15	0.21	0.01	0.08	0.05	0.16	0.42	
ppm																			
Rb	-	-	-	-	-	-	-	21.9	-	6.3	-	13.3	11	36.5	-	27.9	21.9	18.2	
Sr	634	550	692	826	268	935	968	629.3	623	867	599	311	221	157	309	343	234	235	
Cs					1.5	0.3	1.4	0.4	0.7	2	0.6	0.4							
Ba	431	403	331	1658	272	191	458	473	234	507	262	130	548	270	146	230	260	404	
Th	-	-	-	-	-	-	-	4.7	-	6.7	-	3.8	7.4	2.2	-	6.4	2.1	4.5	
U	-	-	-	-	-	-	-	1.1	-	1.2	-	3	1.1	0.8	-	1.5	0.6	0.9	
Zr	47	45	51	54	50	37	91	83	83	103	72	70	98	38	30	138	58	73	
Hf	-	-	-	-	-	-	-	2.4	-	3	2.2	2.8	1.2	3.4	1.5	2.8			
Y	12	10	15	11	10	10	10	13.4	11	14.6	10	13.6	15.9	6.3	11	12.4	18.7	29.4	
Nb	3.8	2.7	5.6	4.3	3.5	5.1	2.2	6.2	12	11.8	5.5	10.9	10.9	3.3	3.1	8.3	3.4	3.9	
Cr	27.37	20.53	20.53	47.89	6.842	61.58	20.53	54.74	41.05	20.53	54.74	75.26	41.05	41.05	102.6	41.05	47.89	34.21	
Co	-	-	-	-	-	-	-	12	-	8	-	17.6	11.2	2.2	-	4.5	15.1	7.3	
Ni	-	-	-	-	-	-	-	16.7	-	9.7	-	28.3	26.7	4.4	-	8.3	6.2	4.4	
Cu	-	-	-	-	-	-	-	19.8	-	56.1	-	75.6	17.3	4	-	8.5	22.1	25.6	
Sc	6	7	10	10	13	14	10	10	10	10	10	11	10	10	20	10	16	11	
V	-	-	-	-	-	-	-	70	-	78	-	222	76	26	-	61	163	82	
La	12.7	-	-	-	-	11.7	-	22.6	23.9	27.4	21.3	23.9	35.4	8.6	-	29.9	9.9	18.8	
Ce	21.3	-	-	-	-	24.4	-	40.1	40.2	49.2	36.6	31.5	55.5	14.1	-	45.7	17.5	31.7	
Pr	2.83	-	-	-	-	2.93	-	4.48	4.93	5.22	4.4	4.67	6.47	1.74	-	5.07	2.19	3.87	
Nd	9.72	-	-	-	-	10.72	-	15.5	15.79	17	14.15	17.6	24.5	6.1	-	17.8	7.7	15.6	
Sm	2.16	-	-	-	-	2.52	-	3.1	2.97	3.2	2.69	2.8	3.6	1.2	-	3.1	2.2	3.4	
Eu	0.76	-	-	-	-	0.78	-	0.82	0.79	0.83	0.96	0.95	1.01	0.41	-	0.72	0.73	0.8	
Gd	2.00	-	-	-	-	2.04	-	2.6	2.57	2.64	2.23	2.55	3.17	1.22	-	1.9	2.45	3.97	
Tb	0.48	-	-	-	-	0.47	-	0.37	0.55	0.43	0.48	0.39	0.47	0.16	-	0.31	0.4	0.64	
Dy	2.12	-	-	-	-	1.89	-	2.17	2.21	2.28	1.9	1.95	2.42	0.91	-	1.73	2.81	3.88	
Ho	0.38	-	-	-	-	0.34	-	0.45	0.4	0.49	0.33	0.46	0.51	0.21	-	0.39	0.61	0.95	
Er	1.31	-	-	-	-	1.12	-	1.22	1.36	1.33	1.13	1.24	1.37	0.66	-	1.17	1.73	2.53	
Tm	0.19	-	-	-	-	0.16	-	0.18	0.2	0.22	0.16	0.18	0.2	0.08	-	0.2	0.27	0.42	
Yb	1.09	-	-	-	-	0.9	-	1.22	1.15	1.28	0.87	1.33	1.42	0.62	-	1.38	1.85	2.56	
Lu	0.16	-	-	-	-	0.14	-	0.19	0.2	0.22	0.14	0.18	0.22	0.07	-	0.21	0.29	0.44	

are aspirated into an ICP mass spectrometer (Perkins-Elmer Elan 6000) for determination of the trace elements, including rare-earth elements (La, Ce, Pr, Nd, Sm, Eu, Gd, Tb, Dy, Ho, Er, Tm, Yb, Lu).

Petrography

The results of the point counts are shown in Table 1. On the basis of the roundness of clasts and quartz contents, the sandstones are generally immature and moderately sorted. The matrix constitutes between 2 and 38 modal % and mainly comprises quartz, plagioclase, chlorite, and clay minerals in the sandstones. Fe-Ti minerals are also significant components as matrix in most of the Upper Cretaceous sandstone. Only one thin section (548) from the Lower Jurassic sandstones has a limonite and/or hematite matrix, and that of 35.2 modal %. Carbonate grains are absent, and they are only a significant component in most of the Lower Jurassic samples as cement. However, mudstone fragments with subordinate fossil shells are also present up to 23 modal % of some of the Upper Cretaceous sandstones (geochemically non-analysed due to their unsuitable modal compositions). Ternary diagrams of detrital modal analyses are usually applied in the classification of sandstones, using the three detrital framework components quartz, feldspar and rock fragments (e.g., McBride 1963; Dott 1964; Dickinson & Suczek 1979; Pettijohn *et al.* 1987). In the present study, all grains having a size between 30–60 μm (silt) were counted as matrix. Depending on the matrix content, two ternary graphs are in use: one for matrix-rich wackes (>15 % matrix), and the other for matrix-poor arenites (<15 % matrix; Dott 1964; Pettijohn *et al.* 1987). In those graphs, chert grains are assigned to the lithic corner. Because in this study the Gazzi-Dickinson method was applied, the QFL plot was selected for sandstone classification.

Seven samples from the Lower Jurassic and thirteen samples from the Upper Cretaceous sandstones can be displayed in the ternary diagram for matrix-rich wackes due to their matrix contents of more than 15 modal %. Feldspar and lithic fragments dominate, whereas quartz fragments are fairly scarce. Thus, samples from the Lower Jurassic sandstones are defined as feldspatic wacke, while samples from the Upper Cretaceous sandstones are defined as lithic wacke (Figure 4a). The remaining samples must be plotted in the ternary diagram for arenites because of their matrix contents less than 15 modal %. Nearly all of the samples from the Upper Cretaceous sandstones plot as lithic arenite, whereas samples from the Lower Jurassic sandstones plot as arkosic arenite (Figure 4b), except for one that falls into the field of lithic arenite.

In the QFL ternary provenance diagram (e.g., Dickinson & Suczek 1979; Dickinson *et al.* 1983), four feldspar-rich sandstones of the Lower Jurassic profile fall into the continental-block field (basement uplift as a subfield for feldspar-rich compositions), while others fall into the transitional-arc field (Figure 4c). The great majority of the Upper Cretaceous sandstones plot in the undissected-arc field except for five that plot in the transitional-arc field, exhibiting a distinct discrimination from the Lower Jurassic samples.

Lithic fragments are the first-order component in terms of abundance of the Upper Cretaceous and the second-order component after feldspar grains in the Lower Jurassic sandstones. Lithic fragments constitute an average of about 30% of the Lower Jurassic sandstones and 47% of the Upper Cretaceous sandstones. In spite of the fact that they are dominated mainly by basaltic and andesitic types in nearly all of the sandstone samples, variable amounts of dacitic and sedimentary fragments are also present. The majority of the basaltic fragments have a brownish or blackish appearence due to decomposition. In large dacitic fragments, anhedral quartz, subhedral to euhedral plagioclase with oscillatory zoning, and amphibole grains within the microgranular matrix are present. Sedimentary fragments are absent in most of the Lower Jurassic sandstones and are more abundant in some of the Upper Cretaceous sandstones, mainly as carbonate fragments and fossil shells.

Feldspar grains are dominated by plagioclase, mostly albitized, and typically show normal to oscillatory zoning. Some feldspar grains have been partially sericitized, and others partially or wholly replaced by calcite. Unaltered small plagioclase grains may be confused with quartz grains. All thin sections were stained for K-feldspar, and the K-feldspar present is entirely orthoclase. Although K-feldspar contents reach significant levels (up to 19%) in sample 338 from the base of the İşhan profile, the Lower Jurassic sandstones generally contain K-feldspar up to 4.4%. On the other hand, K-feldspar generally is absent, although it reaches 4% in some thin sections of the Upper Cretaceous sandstones.

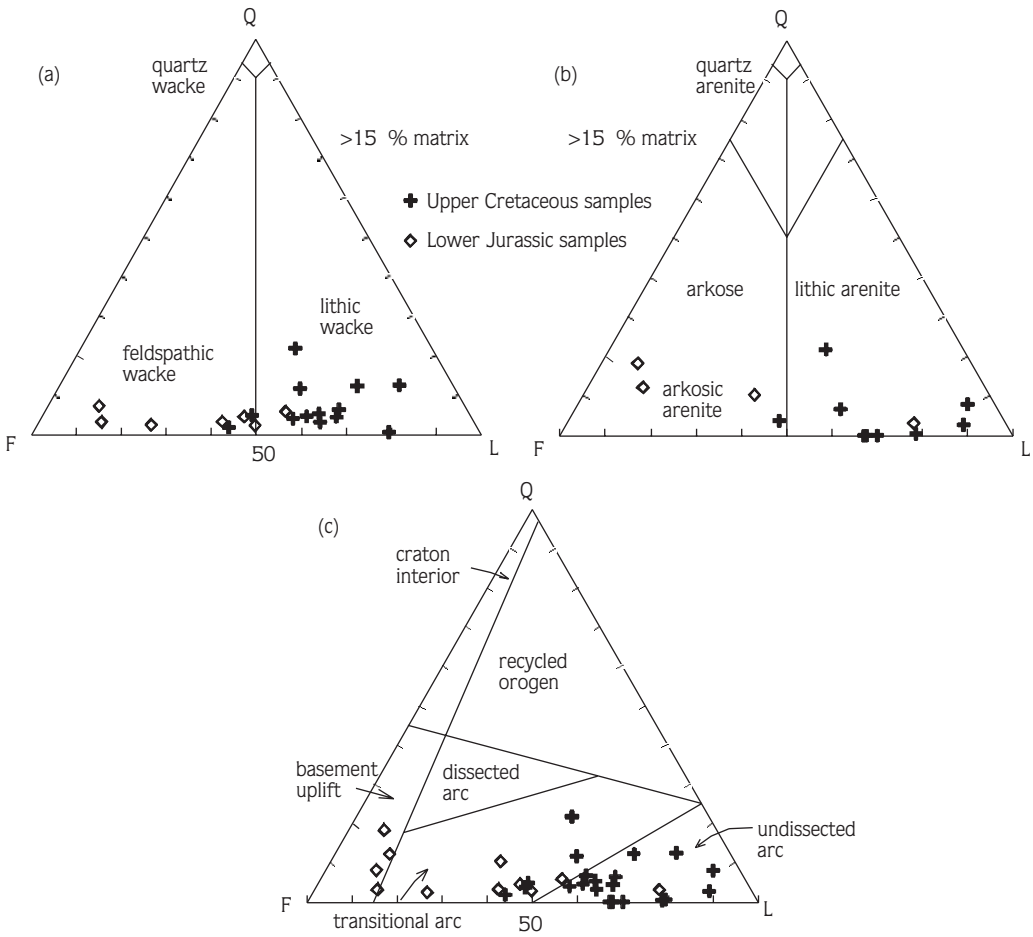

Figure 4. QFL diagrams of Lower Jurassic and Upper Cretaceous sandstones. **Q**– total quartz, **F**– feldspar, **L**– lithic fragments; **(a)** wackes, **(b)** arenites, Koç QFL diagram, with provenance fields, of Dickinson & Suczek (1979).

Quartz is generally quite scarce in both lithologies; only one sample from each profiles has a significant quartz content (up to 19%). Quartz grains typically have a moderate degree of sphericity and roundness, and both monocrystalline and polycrystalline varieties occur though most grains are monocrystalline. Some monocrystalline grains are strained and were most probably derived from plutonic and volcanic rocks. Polycrystalline grains are generally made up of inequant individual crystals. Large polycrystalline grains consist of smaller, elongated individual crystals with smooth or sutured boundaries; such grains are most probably of metamorphic origin.

The bulk heavy-mineral assemblage is in appreciable and is higher in the Upper Cretaceous samples (Table 1); it consists of opaque oxides (i.e., magnetite, ilmenite) and chlorite in decreasing order of abundance. Chlorite occurs in appreciable amounts in some samples. High amphibole contents, up to 18%, were found in the Upper Cretaceous sandstones, an important fact to be considered when interpreting detrital modes and geochemistry in so far as amphibole is sensitive to MREE, HREE and Y. Biotite and muscovite are quite scarce (up to 1.8%) in some of the Lower Jurassic samples.

Geochemistry

Analysed shales and sandstones have been grouped in Table 1 on the bases of age and stratigraphic sections. Likewise, average data for post-Archean shales (PAAS) (Taylor & McLennan 1985), which are considered

representative of the upper continental crust, are included for reference. In addition, correlation coefficients obtained from matrix correlation are reported in Table 2.

Major Elements

The Lower Jurassic and Upper Cretaceous clastic rocks show significant lithological variability, which is reflected in their variation in chemical composition (Table 1); they have commonly overlapping abundances with regard to SiO_2 contents, from 52.4 to 80.6% and 47.9 to 76.2%, respectively, and fall within the greywacke, litharenite, and arkose fields in the chemical classification diagram for the sedimentary rocks (Pettijohn *et al.* 1987; Creaser *et al.* 1997) (Figure 5a). These rocks have broadly similar SiO_2/Al_2O_3 ratios, but variable K_2O/Na_2O ratios (Table 3). However, the low K_2O/Na_2O ratios (<1) in most samples are remarkable with an average ratio of about 1:6; this situation is attributed to a paucity of K-feldspar and biotite. The two points – with an average ratio of 10:1 – represent the shales, reflecting the higher content in K-bearing clay phases and other clay-sized phases compared to sandstones of the same age. Unexpectedly, the shales have higher SiO_2 and lower Al_2O_3, CaO and Na_2O than the associated sandstones (Table 1), except for those in the Kemerlidağ profile which have average values, suggesting the enrichment of fine quartz particles as compared to plagioclase. This behaviour is also supported by the high negative correlation coefficient (r = -0.91) between SiO_2 and Al_2O_3 (Table 2). Generally, the Lower Jurassic rocks tend to have lower $(CaO+MgO)/(SiO_2+K_2O+Na_2O)$ ratios than the Upper Cretaceous rocks (Figure 5b). The rocks show variable degrees of negative correlation of SiO_2 versus TiO_2, MnO, MgO and CaO. There is a positive correlation between Al_2O_3 and TiO_2, indicating chemical weathering in the source area and resulting in a relative concentration of these residual elements. Although the rocks do not exhibit any obvious discrimination in terms of major elements – compared to PAAS (Taylor & McLennan 1985) (Figure 6a) – the Upper Cretaceous sandstones have slightly more depleted patterns for Ti, Fe, Ca and K than their Lower Jurassic equivalents. Low Al values (0.6–0.8 x PAAS) suggest that the source area was not subjected to intense weathering. Na and Ca enrichments accord with their high plagioclase and hornblende contents. However, excessive enrichments in Ca may also be due to the occurrence of some diagenetic calcite cements and increase in the abundance of limestone clasts.

Large-Ion Lithophile Elements (LILEs: Rb, Cs, Ba, Sr)

In comparison with PAAS (Figure 6b), our Lower Jurassic samples generally tend to display more depleted LILE and HFSE patterns. The mean LILE and HFSE concentrations of the fine-grained and coarse-grained fractions from the each units are slightly to moderately depleted, whereas the mean Sr and Nb concentrations are moderately enriched, particularly in the sandstones. These enrichments are in accordance with modally high plagioclase, heavy-mineral (i.e., magnetite, ilmenite) and opaque- cement (i.e., limonite, hematite) contents of certain sandstones. While obvious depletions in the LILE and HFSE contents of the Upper Cretaceous shales relative to associated sandstones are present, their Lower Jurassic counterparts show similarly depleted LILE and HFSE contents. In the Lower Jurassic rocks, Rb, Cs and Ba have moderate to high negative correlation coefficients with Al_2O_3 (-0.64, -0.45 & -0.36, respectively) (Table 2). These correlations suggest that their distributions are not controlled by kaolinitic and montmorillonitic phyllosilicate phases. In contrast, the higher positive linear correlations with K_2O (0.81, 0.75 and 0.44) suggest a strong link to illite and K-feldspar. No correlations have been found between Sr and other elements/oxides, probably due to its occurrence in multiple mineral phases. On the other hand, in the Upper Cretaceous rocks, the LILE have no significant correlations with Al_2O_3, except for Sr and Cs; these have relatively high positive correlation coefficients (0.63 and 0.48), probably indicating that their distributions are mainly controlled by plagioclase.

High-Field-Strength Elements (HFSEs: Zr, Hf, Y, Nb, Ta, Th, U)

High-field-strength element (HFSE) concentrations in the Lower Jurassic and Upper Cretaceous rocks show slightly to moderate positive correlations with TiO_2 and P_2O_5 and negative correlations with Cr, Ni and Sc (Table 2), an expected trend due to their incompatible behaviours. The average Th/U ratio of 5.7 in the Lower Jurassic rocks is higher than in the Upper Cretaceous rocks (3.6), in good agreement with the average ratio of 3.8 in the upper continental crust (Taylor & McLennan 1985). The Th/Sc

Table 2. Correlation coeffcients (r) from the correlation matrix obtained using geochemical data from the shales and sandstones (n= 35). CIA (chemical index of alteration) = [Al_2O_3 / (Al_2O_3+CaO+Na_2O+K_2O)]100.

	Lower Jurassic									Upper Cretaceous							
r	Al_2O_3	K_2O	TiO_2	Zr	Th	Y	P_2O_5	CIA	r	Al_2O_3	K_2O	TiO_2	Zr	Th	Y	P_2O_5	CIA
SiO_2	-0.91	0.29	-0.79	0.02	0.09	-0.22	-0.22	-0.14	SiO_2	-0.38	-0.10	-0.59	0.70	0.56	0.18	0.29	0.61
Al_2O_3	1	-0.47	0.69	0.14	0.17	0.04	0.35	0.18	Al_2O_3	1	-0.22	0.46	0.07	0.06	-0.23	-0.12	0.43
Rb	-0.64	0.81	-0.31	-0.52	-0.12	-0.47	0.33	0.01	Rb	-0.55	0.81	-0.43	-0.13	-0.30	-0.27	-0.25	-0.02
Cs	-0.45	0.75	-0.29	-0.31	-0.01	-0.41	0.36	-0.06	Cs	0.49	0.15	0.11	-0.43	-0.58	-0.45	-0.52	-0.11
Th	0.17	-0.36	-0.12	0.76	1.00	-0.53	0.47	0.66	Th	0.06	-0.65	0.10	0.90	1.00	0.29	0.37	0.61
Ba	-0.36	0.44	-0.29	-0.24	0.16	0.25	-0.45	-0.10	Ba	0.06	0.17	0.28	0.06	0.63	0.06	-0.02	-0.16
U	0.40	-0.60	0.16	0.65	0.51	-0.31	0.42	0.58	U	0.06	-0.46	0.56	0.29	0.26	-0.09	0.02	0.02
Sr	0.10	-0.04	0.28	-0.01	0.13	-0.03	-0.36	-0.10	Sr	0.63	0.07	0.26	-0.09	-0.19	-0.30	-0.25	0.02
Sc	-0.20	0.58	0.20	-0.15	-0.36	-0.06	-0.10	-0.23	Sc	-0.09	-0.21	0.08	-0.25	-0.32	0.12	0.04	-0.04
V	0.37	0.55	0.71	-0.33	-0.10	-0.49	0.13	-0.20	V	0.18	-0.43	0.67	-0.14	-0.22	0.21	0.13	-0.24
Ni	0.26	0.12	0.29	0.19	0.38	-0.47	0.17	0.32	Ni	0.31	-0.52	0.67	0.08	0.23	-0.24	-0.01	-0.05
Co	0.02	-0.38	-0.27	0.29	-0.18	0.60	-0.17	0.06	Co	0.46	-0.45	0.75	-0.20	-0.19	0.12	0.17	-0.14
Cr	0.39	0.08	0.32	-0.21	-0.18	0.31	-0.01	0.52	Cr	0.02	-0.44	0.17	0.08	-0.05	-0.05	0.05	-0.03
Cu	-0.83	0.82	-0.47	-0.31	-0.63	-0.63	-0.04	0.30	Cu	0.31	-0.49	0.34	-0.03	0.02	-0.08	0.02	-0.08
Hf	0.26	-0.59	-0.17	0.89	0.90	-0.27	0.36	0.69	Hf	0.12	-0.63	-0.01	0.92	0.91	0.39	0.44	0.73
Yb	0.09	-0.05	0.00	-0.33	-0.46	0.96	-0.34	-0.61	Yb	-0.26	-0.33	-0.28	0.34	0.28	0.98	0.82	0.15
ΣLREE	0.40	-0.48	0.60	0.46	-0.22	0.35	0.19	-0.58	ΣLREE	0.01	-0.48	0.14	0.68	0.96	0.34	0.35	0.46
ΣMREE	0.25	-0.27	0.27	-0.05	-0.54	0.90	-0.12	-0.57	ΣMREE	0.02	-0.49	0.03	0.48	0.59	0.86	0.89	0.28
ΣHREE	0.03	-0.11	-0.05	-0.28	-0.44	0.96	-0.38	-0.56	ΣHREE	-0.21	-0.30	-0.26	0.29	0.28	0.99	0.85	0.13
$(La/Yb)_C$	0.42	-0.53	0.34	0.57	0.25	-0.46	0.53	0.28	$(La/Yb)_C$	0.24	-0.29	0.47	0.66	0.82	-0.28	-0.04	0.51
$(Gd/Yb)_C$	0.33	-0.42	0.44	0.60	-0.32	-0.44	0.54	0.29	$(Gd/Yb)_C$	0.34	0.04	0.41	-0.10	0.31	-0.40	-0.01	-0.06
La/Sc	0.60	-0.60	0.50	0.36	-0.05	0.18	0.30	-0.27	La/Sc	0.13	-0.47	0.34	0.82	0.95	0.18	0.26	0.55

CIA (chemical index of alteration) = [Al_2O_3/(Al_2O_3+CaO+Na_2O+K_2O)]100

Table 3. Elemental ratios in the analysed groups of shales, sandstones and the PAAS. Only the samples of Table 1, which have full trace-element coverage, are shown in this table.

	Lower Jurassic samples											Upper Cretaceous samples									
	shales						sandstones					shales				sandstones					
	335	339	343	348	538	543	338	349	351	352	PAAS	451	453	580	581	565	569	573	574	576	590
SiO_2/Al_2O_3	11.3	8.4	8.9	4.5	3.2	3.3	6.3	3.0	3.1	3.3	3.3	2.7	3.6	4.3	5.8	3.3	3.7	3.7	4.9	8.8	4.9
K_2O/Na_2O	8.0	13.0	0.1	0.2	0.3	0.3	1.0	0.6	0.6	0.6	3.1	0.3	0.2	0.3	0.4	0.3	0.0	0.2	0.1	1.4	3.3
Zr/Hf	38.8	33.7	34.3	29.9	33.2	32.8	19.6	31.8	32.0	30.1	42	39.3	26.0	38.8	26.0	34.5	34.4	31.8	34.9	31.3	40.7
Zr/Yb	29.1	24.4	33.6	39.3	49.8	79.5	42.6	24.4	15.6	14.3	74.5	33.4	72.8	31.5	28.4	68.0	80.7	52.6	68.7	60.5	100.3
Zr/Th	13.3	33.7	34.3	16.4	20.5	14.0	8.9	22.9	26.0	37.0	14.3	39.3	21.0	27.7	16.2	17.6	15.4	18.4	13.2	17.0	21.6
Th/U	8.8	3.3	4.0	2.3	4.7	6.3	16.8	3.6	4.0	3.3	4.7	1.3	2.2	3.5	5.0	4.3	5.6	1.3	6.7	2.8	4.3
Th/Sc	0.3	0.0	0.3	0.2	0.2	0.9	0.8	0.2	0.1	0.1	0.9	0.1	0.3	0.1	0.4	0.5	0.7	0.3	0.7	0.2	0.6
Co/Th	1.9	5.8	8.9	0.6	3.7	0.7	0.0	5.4	6.5	9.9	1.6	13.9	4.4	7.2	1.6	2.6	1.2	4.6	1.5	1.0	0.7
Cr/Th	1.4	27.4	9.8	1.6	7.3	2.9	3.3	8.2	29.9	31.6	7.5	34.2	13.2	22.8	7.6	11.6	3.1	19.8	5.5	18.7	6.4
Cr/Ni	0.4	4.1	14.4	1.0	1.2	3.7	1.3	2.1	7.5	5.0	2.0	2.2	1.7	7.7	7.8	3.3	2.1	2.7	1.5	9.3	4.9
Cr/V	0.0	0.1	2.3	0.1	0.2	0.2	-	0.2	0.3	0.3	0.7	0.3	0.4	0.3	0.4	0.8	0.3	0.3	0.5	1.6	0.7
V/Ni	11.1	27.5	6.3	18.7	6.9	15.7	0.0	12.9	22.7	17.6	2.7	7.9	4.1	26.3	18.6	4.2	8.0	7.8	2.8	5.9	7.3
La/Sc	0.7	0.3	0.9	0.8	0.7	1.6	0.7	1.3	2.4	1.4	2.4	0.8	0.9	0.6	1.7	2.3	2.7	2.2	3.5	0.9	3.0
La/Th	2.6	6.1	3.6	3.6	2.9	1.9	0.9	6.9	16.5	15.5	2.6	10.5	3.3	4.7	4.2	4.8	4.1	6.3	4.8	3.9	4.7
ΣREE	51.2	35.3	67.0	80.0	67.7	79.3	40.3	85.6	121.0	100.8	185	40.3	40.4	50.6	89.6	95.0	111.7	89.7	136.3	36.1	109.6
ΣLREE	38.5	24.4	45.9	65.2	52.8	66.4	28.2	67.8	100.1	77.3	166	32.0	34.0	37.3	70.0	82.7	98.8	77.7	121.9	30.5	98.5
ΣMREE	9.2	7.7	14.0	10.8	10.6	9.2	7.7	12.6	14.7	16.0	17.6	6.1	4.8	9.2	13.6	9.5	9.9	9.1	11.2	4.1	8.2
ΣHREE	3.6	3.2	7.1	4.0	4.3	3.6	4.4	5.3	6.2	7.5	11.3	2.2	1.6	4.1	6.0	2.8	3.1	2.9	3.2	1.4	3.0
$(La/Sm)_C$	2.4	2.3	2.0	3.0	3.1	4.3	2.8	3.4	4.1	3.1	4.3	3.5	3.9	2.8	3.5	4.6	5.4	5.4	6.2	4.5	6.1
$(Gd/Yb)_C$	1.2	1.2	1.0	1.3	1.3	1.2	0.8	1.2	1.3	1.1	1.4	1.4	1.4	1.1	1.3	1.7	1.7	1.6	1.8	1.6	1.1
$(La/Yb)_C$	3.8	3.0	2.4	5.8	4.7	7.2	2.9	5.0	6.7	4.0	9.2	6.0	7.8	3.6	5.0	12.5	14.5	12.1	16.8	9.4	14.6
Eu/Eu*	0.8	0.9	0.9	0.7	0.8	0.9	1.4	0.8	0.6	0.7	0.65	1.2	1.1	1.0	0.7	0.9	0.8	1.1	0.9	1.0	0.8
CIA	50	48	58	58	59	60	56	43	36	41	70	36	48	45	41	61	54	33	46	25	80

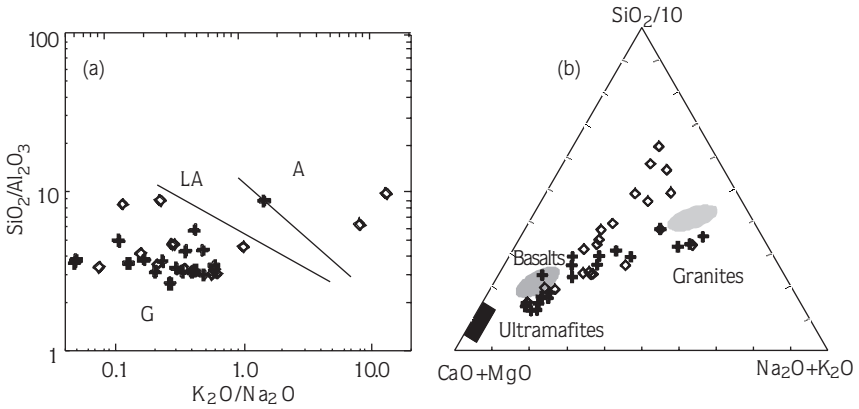

Figure 5. (a) Chemical classification diagram showing the ranges in composition of the Lower Jurassic and Upper Cretaceous shales and sandstones (after Creaser *et al.* 1997; Pettijohn *et al.* 1987). G– greywacke, LA– lithic arenite, A– arkose. (b) $(CaO+MgO)–SiO_2–(Na_2O+K_2O)$ diagram showing comparison between major-element compositions of the analysed samples and those of ultramafites, basalts and granites (after Taylor & McLennan 1985).

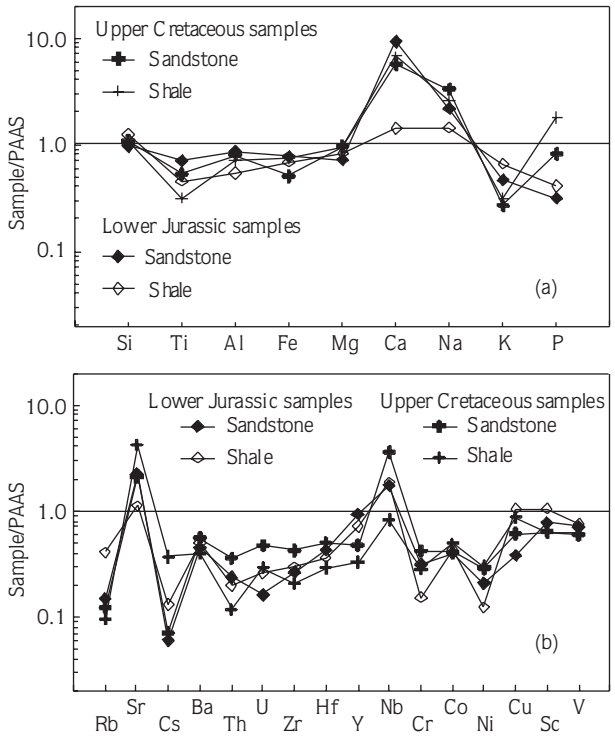

Figure 6. (a) and (b) elemental variations for shales and sandstones of the Lower Jurassic and Upper Cretaceous sedimentary units, respectively from the Yusufeli (Artvin) area. Data are average values normalised to PAAS (Talor & McLennan 1985).

ratio, a good indicator for the bulk composition of the provenance, has average values of 0.30 and 0.39 for the Lower Jurassic and Upper Cretaceous rocks, respectively. For example, the Lower Jurassic and Upper Cretaceous rocks yield a broad relationship between Th/Sc and Zr/Sc that is consistent with provenance-dependent compositional variation (trend 1 in Figure 7). An addition of zircon by sorting and recycling to samples would result in an increase in Zr/Sc ratios, as exemplified by trend 2 in Figure 7. Furthermore, strong positive correlation between Zr and Hf, as attested by their high correlation coefficients (0.89 and 0.92; Table 2), indicate that Th and Zr behave similarly during magmatic differentiation. Also, the choice of coarse-grained rocks in this study increases the possibility that heavy-mineral concentrations might significantly affect the composition of the rocks. Y has strong positive correlation with Yb and heavy-rare-earth elements (HREEs), which seems to reflect that the HREEs are controlled mainly by hornblende abundance. The mean Y contents are lower in the Upper Cretaceous rocks (12.5 ppm) than in the Lower Jurassic rocks (17.6 ppm), having contents similar to the PAAS (27 ppm). In addition, the negative correlation between Y and SiO_2 in the Lower Jurassic rocks seems to reflect its association with minerals preferentially concentrated in quartz-poor rocks.

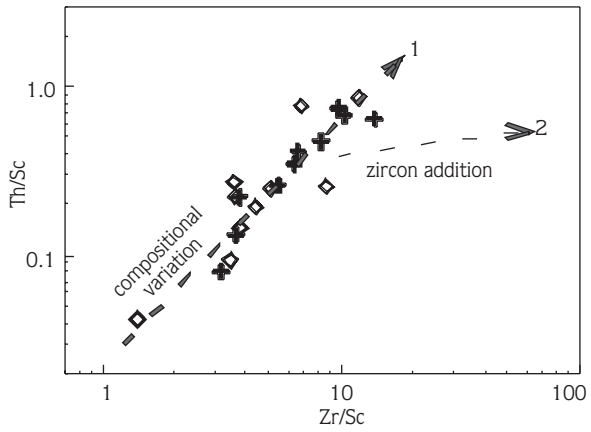

Figure 7. Th/Sc vs Zr/Sc variation plot for sedimentary rocks of the Yusufeli area. The compositional variation trend line (1) was defined by McLennan *et al.* (1993) for sedimentary rocks from active margins that are least affected by sedimentary sorting and recycling. Zircon accumulation by sorting and recycling would result in Zr enrichment relative to Th, defined by trend line (2) (McLennan *et al.* 1993).

Transition Trace Elements (TTEs: Cr, Co, Ni, Cu, Sc, V)

As observed for the great majority of the other trace and major elements, the transition trace-element (TTE) contents of the studied shales and sandstones are also depleted relative to those of the PAAS (Figure 6b), with the exception of the Cu and Sc values for the Lower Jurassic shales, which have patterns quite similar to the PAAS. These rocks have low Cr and Ni contents (and Cr/Ni ratios in general), demonstrating the absence of ultramafic rocks in the source area. However, the higher concentrations of Cr (42 ppm on average) in the Upper Cretaceous sandstones with respect to those in the Lower Jurassic rocks (26 ppm on average) indicate a higher proportion of mafic rocks in their source area (Taylor & McLennan 1985; Wronkijewicz & Condie 1987). The Cr/Th ratio, a good indicator for provenance (Condie & Wronkiewicz 1990), has average values of 12 and 14 in the Lower Jurassic and Upper Cretaceous rocks, respectively (Table 3). In general, all of the TTEs in the Upper Cretaceous sandstones are positively correlated with TiO_2 and Al_2O_3 (Table 2), indicating that they are mainly concentrated in the heavy minerals and phyllosilicates. In contrast, there are no systematic correlations between the TTEs and TiO_2 and Al_2O_3 in the Lower Jurassic shales and sandstones, suggesting that additional factors also control their distribution.

Rare-Earth Elements (REEs)

Chondrite- and PAAS-normalized REE patterns are given in Figures 8 and 9. Although the total REE contents and the magnitude of LREE-enrichment and Eu anomalies vary, the patterns for the Lower Jurassic and Upper Cretaceous rocks are broadly similar to one another, and to the PAAS (Figure 8). The Lower Jurassic shales seem to have lower REE contents in comparison to associated sandstones. In general, they are characterized by low $(La/Yb)_C$ ratios (<7 except for sample 543 with a value of 7.2), and slight to moderate negative Eu anomalies (Eu_c/Eu_c^* = 0.57–0.94), except for a high positive Eu anomaly (Eu_C/Eu_C^* = 1.42 in sample; Table 3). Although all the mean REEs are depleted relative to the PAAS (Figure 9a), depletions in the LREE concentrations are greater than the mean HREE concentrations, with the exception of the mean REE concentration of sandstones from the Kemerlidağ profile, which show roughly a flat REE pattern. If LREE, MREE and HREE are separately considered, all show strong positive correlation with Y (r = 0.92; Table 2), although the LREE and MREE show

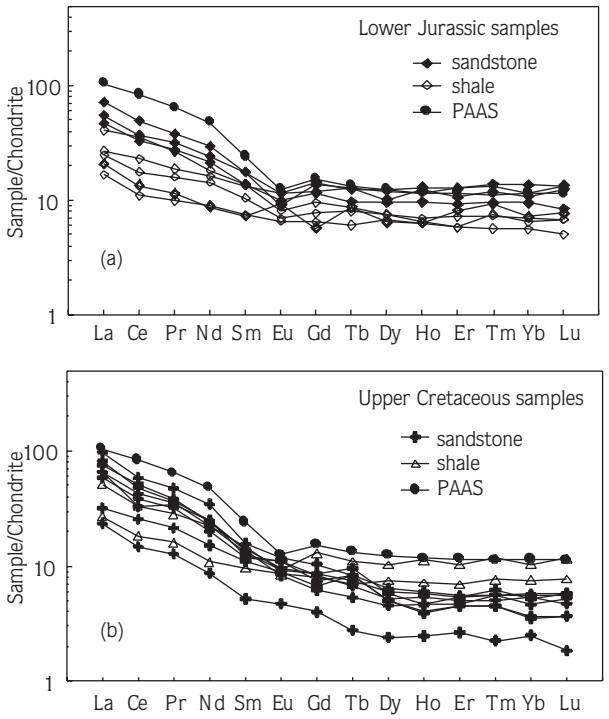

Figure 8. Chondrite-normalised REE patterns of shales and sandstones of Lower Jurassic and Upper Cretaceous age from the Yusufeli area. The PAAS pattern is given for reference.

slightly to moderately positive correlations with Al_2O_3, TiO_2 and Zr. All of these correlations seem to indicate that – in addition to hornblende – various mineral phases, such as phyllosilicates, opaque phases and zircon, have played some role in controlling the REE contents.

The Upper Cetaceous rocks have highly enriched LREE patterns (La_C/Sm_C = 2.83–6.18), and flat to moderately fractionated HREE patterns (Gd_C/Yb_C = 1.07–1.83) (Figure 8b; Table 3). The samples are characterized by slightly negative to moderately positive Eu anomalies (Eu_C/Eu_C^* = 0. 7–1.17). The total REE contents are lower in the Upper Cretaceous rocks (average ΣREE = 87 ppm) than in the Lower Jurassic rocks (average ΣREE = 93 ppm). Compared to the PAAS (Figure 9b), the mean REE contents exhibit flat but depleted patterns, except for the mean REE contents of shales from the Çağlayan profile, which are similar in appearance to the PAAS. Y and P_2O_5 show moderate to high positive correlations with MREE and HREE (Table 2). In addition, Zr and Th show strong positive correlations with LREE and MREE. All of these correlations indicate that REE distribution is likely controlled by the collective influence of hornblende, zircon, phosphates and opaque phases.

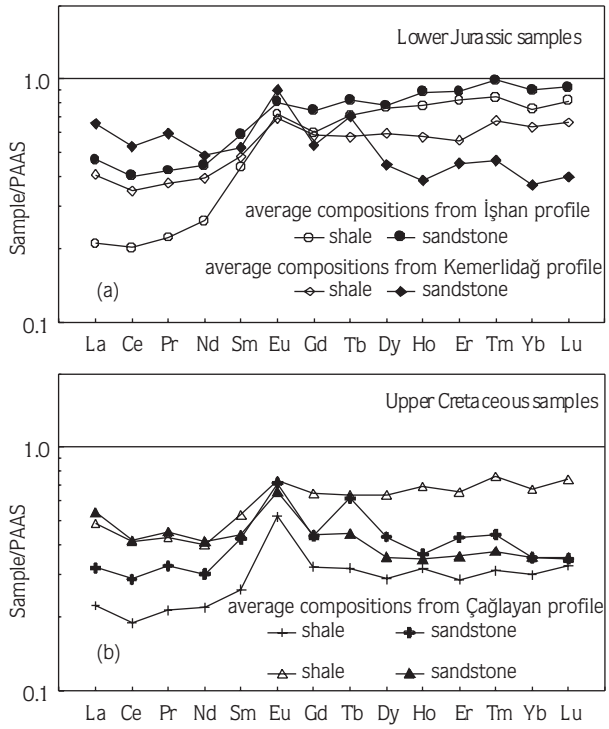

Figure 9. PAAS-normalized distribution of selected trace elements in average Lower Jurassic and Upper Cretaceous shales and sandstones. PAAS-normalising values are from Taylor & McLennan (1985).

Discussion and Interpretation

Provenance

The major- and trace-element compositions of the two units overlap, but nevertheless are distinct enough to suggest that the bulk compositions of their source regions were slightly different. The relative abundance of modal plagioclase in the Lower Jurassic rocks is the principal difference between them and the Upper Cretaceous rocks, represented by lithic arenite and lithic wacke petrofacies. The Lower Jurassic samples are scattered in the transitional-arc and basement-uplift fields, while the Upper Cretaceous samples mainly fall in the undissected-arc field of Dickinson & Suczek (1979) (Figure 4c). In all samples from these units, quartz is dominantly monocrystalline, suggesting an igneous source for the majority of the material. The paucity of polycrystalline quartz and sedimentary lithic fragments (fossil shells excluded), and the abundance of basaltic and dacitic fragments, suggests that these feldspathic and lithic arenites and wackes were derived from a volcanic source where basic and acidic rocks were exposed and altered through chemical and physical weathering during a single cycle of sedimentation. Thus, the most likely source terrain for these rocks would be volcanic rocks older than Early Jurassic, possibly Late Palaeozoic, which are no longer exposed/present (Yılmaz 1972; Bergougnan 1987).

Plots of relatively insoluble elements in waters as ratios, such as Th/Sc, La/Sc, Co/Th, Cr/Th, Cr/V, V/Ni and Cr/Ni, are good indicators of provenance (McLennan *et al.* 1983, 1990; Taylor & McLennan 1985; Wronckiewicz & Condie 1989, 1990; Cullers 1994), and help to elucidate concentration or dilution effects of sorting during sediment transport. The trace-element data from these units were plotted on a Sc-Th crossplot in two fields (Figure 10a). One field is characterized by a Th/Sc ratio near 1, typical of continental crust that is enriched in incompatible elements. The other field is characterized by an enrichment in Sc (Th/Sc <1), usually found in more mafic sources that are enriched in compatible elements. The trace-element composition of each unit results from variable mixing of sediments deposited at each location. The contributions from each source are similar for the two units in so far as they are controlled by geographic proximity to each source. Figure 10b is an element-ratio plot of Th/Sc vs. Cr/Th. This plot varies in contrast with different proportions from continental and mafic sources; also drawn in Figure 10b is a curve that best fits the data.

This curve is consistent with a two-component mixing model between felsic and mafic end-members. It seems apparent that at least two source areas were involved in providing detritus to the basin during deposition of the units. The dominant source has a mafic signature, with some of the cratonic material less felsic than average continental crust. The signatures of the felsic enrichment over upper crust – represented by highly evolved alkaline igneous rocks – and mafic enrichment close to MORB are not indicated. The relatively low Cr/Ni ratios from both shales and sandstones of each unit provide no evidence of significant amounts of ultramafic lithologies in the source area. The relative abundance of Cr and Ni contents in the Upper Cretaceous rocks compared to the Lower Jurassic rocks has been interpreted to reflect unroofing of upper crust. In general, values of Zr/Hf, Th/Sc, La/Sc, Th/Sc, La/Yb ratios and CIA are lower and values of Co/Th, Cr/Th, V/Ni and Cr/Ni ratios are higher in the shales and sandstones of each unit compared to those of the PAAS (Table 3). All of these ratios indicate a more basic source than the upper crust; therefore, they are close to those of mid-continental crust. Table 4 gives elemental ratios of different igneous and sedimentary materials; these indicate that the shales and sandstones of the Yusufeli area have values similar to those the andesites of Condie (1993), and lie between sands derived from basic and acidic rocks (Cullers *et al.* 1988; Cullers 1994). As a result, it is suggested that the contribution of

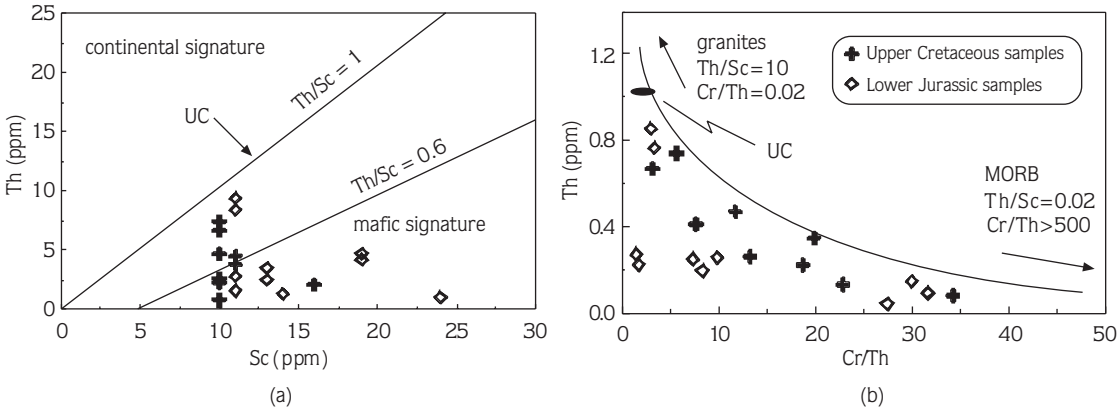

Figure 10. (a) Th vs Sc for the Lower Jurassic and Upper Cretaceous samples. Th is an incompatible element that is enriched in felsic rocks, and Sc is a compatible element that is enriched in mafic rocks. Th/Sc ratios near unity are typical of upper continental-crustal (UC) derivation, and Th/Sc ratios near 0.6 suggest a more mafic component. (b) Th/Sc vs Cr/Th for the samples. The samples lie on the lower side of a curve consistent with mixing of a continental source enriched in incompatible elements (Th) and a more mafic source enriched in compatible elements (Cr and Sc). Values for average upper continental crust (UC), average granites, and average mid-ocean-ridge basalts are given for comparison.

Table 4. Elemental ratios typical of granites, andesites, ophiolites, and sands from basic and silicic rocks, the upper continental crust (UCC), lower continental crust (LCC) and oceanic crust (OC), and from terrigenous rocks of the Yusufeli area reported in this study.

Elemental Ratio	granites[a]	andesites[a]	ophiolites[b]	sand from basic rocks[c]	sand from felsic rocks[c]	UCC[d]	LCC[d]	OC[d]	shales[e]	sandstones[e]
La/Sc	8.0	0.9	0.25	0.4–1.1	2.5–16	2.7	0.30	0.10	0.66	1.46
Sc/Th	0.28	4.65	56	20–25	0.05–1.2	1.0	34	1.73	5.00	3.34
Cr/Th	0.44	9.77	410	22–100	0.5–7.7	3.3	222	1227	10.04	18.24
Co/Th	0.17	4.65	70	7.1–8.3	0.22–1.5	0.9	33	214	4.30	5.46
Eu/Eu*	0.34	0.66	1.0	_	_	0.61	1.07	1.02	0.83	0.88

[a] Condie (1993)
[b] Spadea et al. (1980)
[c] Cullers (1994); Cullers et al. (1988)
[d] Taylor & McLennan (1985)
[e] This study

intermediate and basic rocks rather than acidic rocks to the the sedimentation seems to have predominated.

A more distinct discrimination between the source areas of the units may be inferred by using REE characteristics. The Lower Jurassic shales and associated sandstones have moderately fractionated REE patterns, with average La_C/Yb_C values of 3.7 and 7.9, and negative Eu anomalies (Eu_C/Eu_C^* = 0.8 and 0.9 on average), respectively. Sample 338 is an exception with its moderately positive Eu anomaly (Eu_C/Eu_C^* = 1.4), which is due to its high K-feldspar and plagioclase contents (Table 1). The average LREEs are moderately fractionated (La_C/Sm_C = 2.4 and 4.0), and the HREE patterns are almost flat (Gd_C/Yb_C = 1.2 & 1.3, respectively) (Figure 8a). These characteristics indicate that the original source area for the Lower Jurassic rocks was felsic, and the negative Eu anomalies are regarded as evidence of a differentiated source, possibly similar to dacite or rhyolite (Taylor & McLennan 1985; Slack & Stevens 1994). On the other hand, depletions in K_2O, Rb and Cs, and enrichments in Na_2O, CaO and Sr in comparison with PAAS (Figure 6a & b) suggest the occurrence of plagioclase-rich rocks rather than K-feldspar-rich rocks in the source area. In addition, depleted REE patterns in comparison with PAAS (Figure 9a) reflect a greater contribution from intermediate rather than felsic rocks. Therefore, they plot near shales and sands originated from mid-continental crust.

The REE patterns of the Upper Cretaceous samples are highly fractionated (La_C/Yb_C = 6.0–16.8), with slightly negative to positive Eu anomalies (Eu_C/Eu_C^* = 0.8–1.2), except for the two shale fractions which are characterised by moderate REE fractionation (La_C/Yb_C = 3.6 and 5.0) and negative to neutral Eu anomalies (Eu_C/Eu_C^* = 0.7–1.0) (Table 3; Figure 8b). The LREEs and MREEs are also moderately fractionated (La_C/Sm_C = 2.8–6.9, Gd_C/Yb_C = 1.1–1.8) and HREE enrichment is lower than that of the Lower Jurassic rocks. These features suggest that the source area was geochemically similar to that of the Lower Jurassic rocks in general, but contributions from less or moderately evolved rocks seems to have been more widespread. The marked positive CaO, Sr and Eu anomalies in the PAAS-normalised diagrams (Figure 6a & b) indicate a pronounced contribution of moderately evolved and even mafic materials to sedimentation. Compared to the PAAS, the relatively flat and depleted REE patterns (Figure 9b) reflect the abundance of low to moderately evolved calc-alkaline materials in the modal mineralogical content.

Mineralogical Control and the Effect of Sedimentary Processes on REE Distribution

In the Lower Jurassic rocks, depletions in LREE against HREE (Figure 9) imply that the concentrations of the LREEs in these rocks were provided by an abundance of low total-REE-bearing minerals, such as quartz and plagioclase. These features of the shales and associated sandstones are consistent with their relatively high silica and alumina contents, respectively (Table 1). Strong positive correlations between Y and HREE (r = 0.96) and MREE (r = 0.90) (Table 2) indicate that control on these elements was supplied mainly by hornblende. But LREE-enriched and HREE-flat patterns in the chondrite-normalised plot (Figure 8) rule out hornblende control on REE distribution as the sole factor. Strong positive correlation between Zr and Th (r = 0.76) implies that the contents of both elements may have been derived from zircon. However, the mean Zr contents of the shales are similar to those of associated sandstones, indicating that this mineral was not preferentially concentrated and/or did not exert a strong influence on Zr and Th distributions. Moreover, although zircon accumulation usually causes marked enrichment in LREEs, poor negative correlation of Zr with LREEs (r = -0.33) indicates that zircon has little or no influence on the abundance of these elements. Slight to moderate positive correlations between LREE and Al_2O_3 and TiO_2 (r = 0.40 and 0.60) suggest the compound influence of plagioclase, Ti-bearing minerals (such as biotite, ilmenite, titaniferous magnetite) and clay minerals (in addition to hornblende) present in the sediments rather than a selective effect of one of these minerals.

In the Upper Cretaceous rocks, the moderate positive correlations between LREEs and Zr (r = 0.68) and Th (r = 0.96) (Table 2) suggest that LREE enrichment was produced by the occurrence of zircon and opaque minerals. In addition, positive correlations of Y with Yb and HREEs (r = 0.98 & 0.99, respectively) and positive correlations of P_2O_5 with Yb, MREEs and HREEs (0.82, 0.89 & 0.85, respectively) indicate that hornblende and phosphate played important roles in the distribution of MREEs and HREEs; this observation is supported by the modal compositions of certain sandstones, which include

varying amounts of hornblende. Slight to moderate correlation of CIA with LREEs and MREEs (r = 0.46 & 0.28, respectively) also indicate the influence of opaque cement present in some of the Upper Cratecous sandstones. These sandstones generally are characterised by positive Eu anomalies, indicating the abundance of basaltic fragments which themselves contain abundant plagioclase laths.

Transportation, hydraulic sorting and deposition may significantly affect the chemical compositions of terrigenous sediments, controlling the distribution of major elements (P_2O_5 and TiO_2) and some trace elements (e.g., REE, Th, U, Zr, Hf & Y); therefore, these elements may not be representative of provenance if heavy-mineral concentrations affect the elemental distributions (cf. Reimer 1985; Cullers *et al.* 1987; McLennan 1989).

In the Lower Jurassic sediments, there is a strong textural dependency upon chemical composition. SiO_2, K_2O, Zr and Rb contents are enriched, whereas Al_2O_3, MgO, CaO, Cr, Ni and particularly REE are depleted in shales relative to associated sandstones (Table 1). These elemental distributions suggest the existence of a relatively high energy level, which impeded the accumulation of clay-sized sediments during deposition of the shales. Moreover, the shales yield a more depleted LREE pattern on average relative to associated sandstones in the PAAS-normalized plot (Figure 9), thus supporting the argument for enrichment of silt-sized quartz during sedimentation; this is because quartz has low total REE contents even though it gives an LREE-enriched pattern against HREE on REE-normalised diagrams (Götze 1998). Shales have depleted CaO and Na_2O values relative to associated sandstones (Figure 6a) thus demonstrating the influence of hydraulic sorting and degree of recycling on the chemical composition of terrigenous sediments. All of these differences between the shales and sandstones indicate that sedimentary sorting was an important process that controlled the chemical composition of these clastic rocks.

The Upper Cretaceous sandstones yield highly fractionated REE patterns with $(La/Yb)_C$ values ranging from 6.0 to 16.8, and slightly positive to negative Eu anomalies (Eu/Eu* = 0.8–1.1) (Table 3). When the abundance and angular shape of lithic fragments are taken into consideration, these features can be interpreted as reflecting the influence of the REE characteristics of the source area on sandstone chemistry, which may have resulted from a single cycle of sedimentation. In general, shale fractions that have low $(La/Yb)_C$ ratios (3.6–7.8) and negative Eu anomalies may be regarded as reflecting the homogenized effects on the REEs of hydraulic sorting, chemical weathering and/or degree of recycling.

Subaerial Weathering

Variable degrees of weathering in source areas may have an important influence on the abundances of alkalis and alkaline-earth elements in siliciclastic sediments. Cations such as Rb and Ba are often fixed in weathering profiles, whereas cations with smaller ionic radii – such as Na, Ca and Sr – are more rapidly removed from weathering profiles as dissolved species (Nesbitt *et al.* 1980). A common approach to quantifying the degree of source-area weathering is to use the chemical index of alteration (CIA; Nesbitt & Young 1982). This index can be calculated using molecular proportions

$$CIA = [Al_2O_3/(Al_2O_3+CaO^*+Na_2O+K_2O)]$$

where CaO* is the amount of CaO incorporated in the silicate fraction of the rock.

CIA values for the Lower Jurassic shales and associated sandstones range from 36 to 60 (Table 3), with an average of 53, a value typical of moderately weathered rocks. The Upper Cretaceous rocks have CIA values of 25–61, with an average of 46 (excluding sample 590, which has an unusually high CIA value of 80), indicating a low degree of chemical weathering in the source area. Compared with the PAAS, these shales and sandstones are enriched in Ca, Na and Sr, whereas K, Cs Rb, Ba are depleted (Figure 6a & b). This result is at odds with studies by Nesbitt *et al.* (1980) and Wronkiewicz & Condie (1987), in which they conclude that smaller cations are selectively leached, whereas cations with relatively large ion radii have been fixed by preferential exchange and adsorption on clays. Therefore, in general, weathering conditions were not more intensive in the primitive source areas(s) of the shales and sandstones than that/those of the PAAS. A distinct increase in the clay/sand ratio upwards in the Lower Jurassic sequences may suggest erosion of an intensely weathered source area and a lessening of tectonic activity, and/or a gradually decreasing subsidence rate. There is also an increase in CIA values stratigraphically upwards (CIA = ~ 60), suggesting an increase in the amount of weathering

or a decrease in the erosion rate of the source terrain.

The Upper Cretaceous rocks have CIA values that generally decrease stratigraphically upwards. Initially high values from the Ormandibi profile (CIA = 61) may reflect erosion of a deeply weathered source terrain during deposition of the basal sediments. With increasing tectonic activity, relatively unweathered source material may have commenced to enter the basin, resulting in a decrease in CIA values in the Ormandini sequence (CIA = 25). However, the existence of some red carbonate and silty to clayey horizons (up to 170 m in thickness) within the succession suggest that tectonic and/or volcanic activity waned, resulting in decreased erosion rates and increased input of chemically weathered material into the basin. This may explain the increase in the CIA value of sandstone sample 590 (CIA = 80) in the Ormandibi profile.

On the other hand, the red colour of these sediments may have originated from volcanic activity of the palaeo-Pontian arc, just north of the basin, during the Late Cretaceous. However, this probability seems to be ruled out in so far as this kind of colouration derives from solutions rich in Fe, Mg, Mn and Ti and has no effect on the CIA indices of the sediments since the CIA formula does not use any of these elements. The effects of hydraulic sorting and transportation on CIA indices is also ruled out in so far as these processes mainly influence physical weathering. However, it seems possible that selective enrichment of a mineral (using one or two components of the CIA formula – such as plagioclase, K-feldspar, corundum and calcium phosphates) occurs during transportation. Such an obvious enrichment is reflected only in the SiO_2 contents and SiO_2/Al_2O_3 ratios (Table 1 & 3) of the Lower Jurassic shales relative to the associated sandstones, indicating that enrichment occurred more in the quartz content of the shales than in their plagioclase and K-feldspar contents. Additionally, the abundance of angular components, particularly in the Upper Cretaceous sandstones, demonstrates that no selective enrichment in the modal percentages of any mineral has occurred along the transport path. Consequently, the tendency for increase in the CIA indices of the red Upper Cretaceous sediments may be attributed, at least during some time periods, to increases in the rate of chemical weathering in the source area(s) prior to intense erosion.

On the Al_2O_3–(CaO^*+Na_2O)–K_2O (A-CN-K) diagram (Figure 11) of Nesbitt & Young (1984, 1989), the Lower Jurassic and Upper Cretaceous rocks, as expected, define a linear array along the A-CN join. Two shale samples from the Lower Jurassic rocks plot away from the expected weathering trend of mafic rocks along the A-CN join. Similar trends have been observed in ancient weathering profiles (Grandstaff *et al.* 1986; Nesbitt & Young 1989) and in Archean shales, such as those of the Buhwa Greenstone Belt (Fedo *et al.* 1996), and are interpreted to be a result of K-metasomatism, reflecting either peculiar soil-forming processes in the Precambrian or post-depositional alteration (Kimberley & Holland 1992). Data from the Upper Cretaceous profile plot on the A-CN join at ~ 80, which may be attributed to relatively intense chemical weathering of the source area during some periods. Degree of chemical weathering is mainly a function of climate and rate of erosion, the latter of which is controlled by relief and vegetative cover in the source area. Assuming high erosion rates (as indicated by the abundance of coarse detritus in the Upper Cretaceous sediments) – due to the tectonically active setting of the basin and the degree of weathering – a lack of vegetation at least during some periods of the Late Cretaceous and a strong influence of climate on chemical weathering are

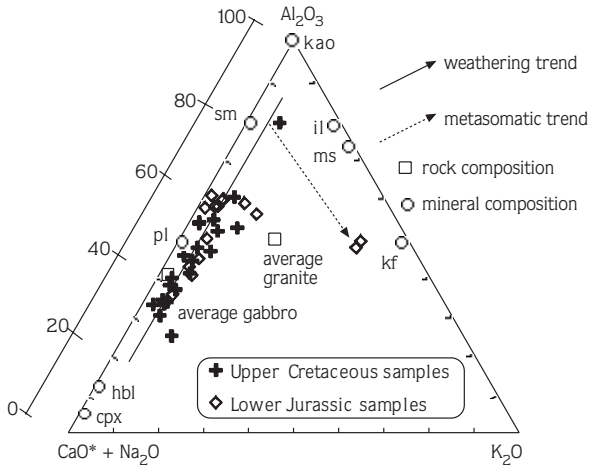

Figure 11. Al_2O_3–(CaO^*+Na_2O)–K_2O (A-CN-K) diagram of the Lower Jurassic and Upper Cretaceous shales and sandstones (compositions as molar proportions, CaO* represents CaO of the silicate fraction only). Selected rock and mineral compositions and weathering trends (after Nesbitt & Young 1984) are given. **Kao**– kaolinite, **il**– illite, **ms**– muscovite, **kf**– alkali-feldspar, **sm**– smectite, **pl**– plagioclase, **hbl**– hornblende, **cpx**– clinopyroxene; average granite and gabbro from Nesbitt & Young (1984).

suggested. Severe weathering may have been related to a CO_2-rich atmosphere and/or elevated surface temperatures; an arid climate may thus be postulated for the Upper Cretaceous in the source area (e.g., Young 1991; Kasting 1993; des Marais 1994).

Tectonic Setting

Plate-tectonic setting discrimination of ancient sedimentary basins are usually accomplished using major- and trace-element bivariate and multivariate plots. Although such graphs are not really significant for specific local plate-tectonic settings, some correlations between tectonics and geochemical processes in sandstones, as well as the relationships among and temporal and spatial variations within various lithostratigraphic units, can be evaluated.

The ratio of SiO_2 vs K_2O/Na_2O provides a tectonic-setting discriminator for sandstone-mudstone suites (Roser & Korsch 1986). In Figure 12a, the investigated samples plot mainly in the fields of arc and active continental-margin settings. The samples plotting in the passive-margin setting represent quartz- and phyllosilicate-rich shales of Early Jurassic age that show similar patterns in most of the following tectonic-discrimination diagrams. A similar plot using the SiO_2/Al_2O_3 ratio instead of SiO_2 discriminates the sandstones and mudstones of different settings (Maynard *et al.* 1982) (Figure 12b). In this plot, the investigated samples mainly group in the arc field due to their low SiO_2/Al_2O_3 and K_2O/Na_2O ratios, and can be separated into two categories: A_1 (<10 % Q, basaltic and andesitic detritus) and A_2 (higher Q, acidic volcanic detritus). Shales that are mineralogically mature (quartz-rich) scatter in the active continental-margin and passive-margin fields, as seen in the graph of SiO_2 vs K_2O/Na_2O. Two ternary plots, in which the highly incompatible trace elements Th and Zr are plotted against the highly compatible elements Co and Sc, have been used (Bhatia & Crook 1986) (Figure 12c & d). The analysed samples plot in the fields for oceanic island arc and continental island arc, with generally high Zr/Th ratios and moderate abundances of Co and Sc. Two shale samples from the Lower Jurassic rocks plot outside the fields on the Th-Co-Zr/10 plot due to their low Co contents; this situation is probably due to depletion of ferromagnesian minerals and basaltic fragments and increased abundance of quartz during sedimentary processes. In general, there is a distinct overlap, albeit with slight difference, of the compositions of the Lower Jurassic and Upper Cretaceous units. Another important point to note is that with decreased grain size (e.g., the shales), the samples show a tendency to fall into the passive-margin field. The reason for this is the 'grain-size effect' on chemical composition. Roser & Korsch (1985) found that the modal and chemical compositions of greywackes and argillites are strongly controlled by grain size. As mean grain size decreases in transition from sandstone to argillite, modal quartz, feldspar and lithic fragments decline in abundance and modal matrix and phyllosilicate correspondingly increase; this strongly affects bulk chemistry. SiO_2 and Na_2O decrease regularly from sandstone to argillite, and K_2O increases. These changes produce a progressive increase in K_2O/Na_2O ratio with decreasing SiO_2. As for the Lower Jurassic shales, they also display higher K_2O/Na_2O ratios relative to associated sandstones, except for higher SiO_2 contents which are undoubtedly related to their unexpectedly high quartz contents, as mentioned above.

Evolution of the Basin

Data from the sandstones and shales of the Yusufeli area, when considered in conjunction with sedimentological, structural and geodynamic data given in earlier papers, allow a reconstruction of the sedimentological and tectonic events in the Yusufeli area from the earliest Jurassic to present. In light of all of these data, it is proposed that the basin evolved from a rifted margin to a passive margin (Şengör &Yılmaz 1981; Bektaş *et al.* 1984; Koçyiğit *et al.* 1992; Ustaömer & Robertson 1993; Yılmaz *et al.* 1997; Okay & Şahintürk 1977; Adamia *et al.* 1997; Dean 2005), and then to a foreland basin (Koçyiğit 1991; Tüysüz *et al.* 1995; Yılmaz *et al.* 1997; Okay & Şahintürk 1997) prior to complete closure. Sedimentary detritus that contributed to each unit was not only derived from the crystalline basement but, also, and more significantly, from the volcanic rocks of a Late Palaeozoic arc. Figure 13 shows a summary and chronology of events for the Mesozoic basin in the Yusufeli area. Each stage of this basin's evolution is represented by a lithological sequence comprising a number of rock units. On the basis of the sedimentary architecture, the depositional history of this basin can be divided into four stages.

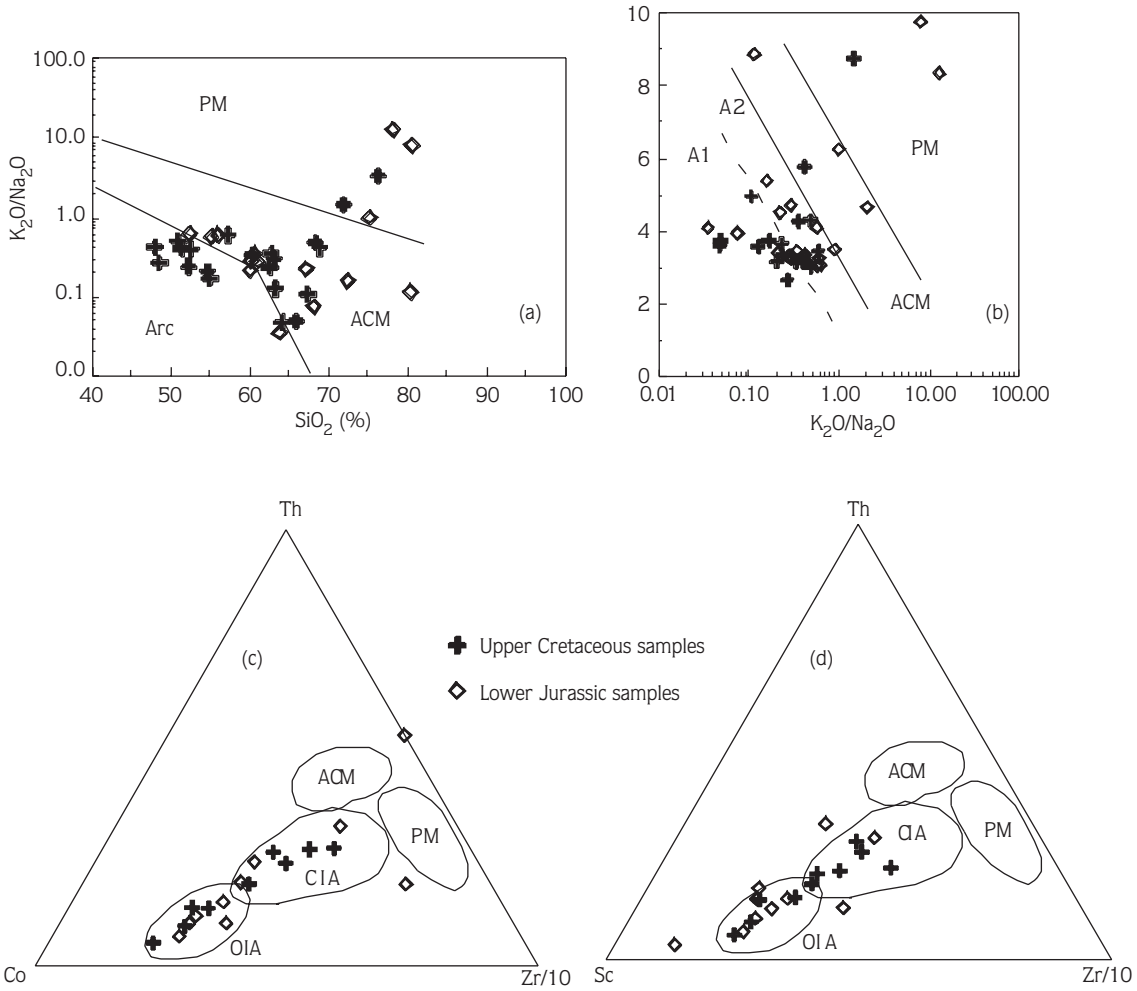

Figure 12. Plot of samples from the Yusufeli area on tectonic discrimination diagrams in order to distinguish sources for the sedimentary rocks. **(a)** SiO_2–Log K_2O/Na_2O diagram of Roser & Korsch (1986), and **(b)** SiO_2/Al_2O_3 vs. K_2O/Na_2O diagram of Maynard *et al.* (1982). On both diagrams, sandstone samples fall in the fields for arc and active continental-margin settings, whereas some of the shale samples fall in the field for a passive-margin setting which is caused by grain-size effects on the chemical compositions of the rocks. As the grain size reduces, the phyllosilicate abundance correspondingly increases in the transition from sandstones to shales (Roser & Korsch 1985). **(c)** Th-Co-Zr/10 and **(d)** Th-Sc-Zr/10 diagrams reported by Bhatia & Crook (1986). **PM**– passive margin, **ACM**– active continental margin, **CIA**– continental island arc, **OIA**– oceanic island arc, A_1– arc setting, basaltic and andesitic detritus, A_2– evolved arc setting, acidic volcanic detritus.

The earliest stage was characterised by the break-up of an arc during Early Jurassic time in which syn-rift sequences, including the Hamurkesen formation and equivalent basic volcanic rocks along the southern margin of the arc, accumulated. During this break-up, rifting is envisaged to have taken place not only along the southern margin of the arc but also in the interior of Neotethyan basin to the south, forming a series of intra-arc rifts parallel to the continental margin, which later evolved to form grabens or half grabens (Şengör *et al.* 1980; Şengör & Yılmaz 1981; Bektaş *et al.* 1984; Tüysüz 1990; Yılmaz *et al.* 1997; Okay & Şahintürk 1997).

The transition from a rifted to a passive margin is represented by the deposition of first marine sediments (after coal-bearing non-marine sediments) above an unconcormity, upon which the lowermost part

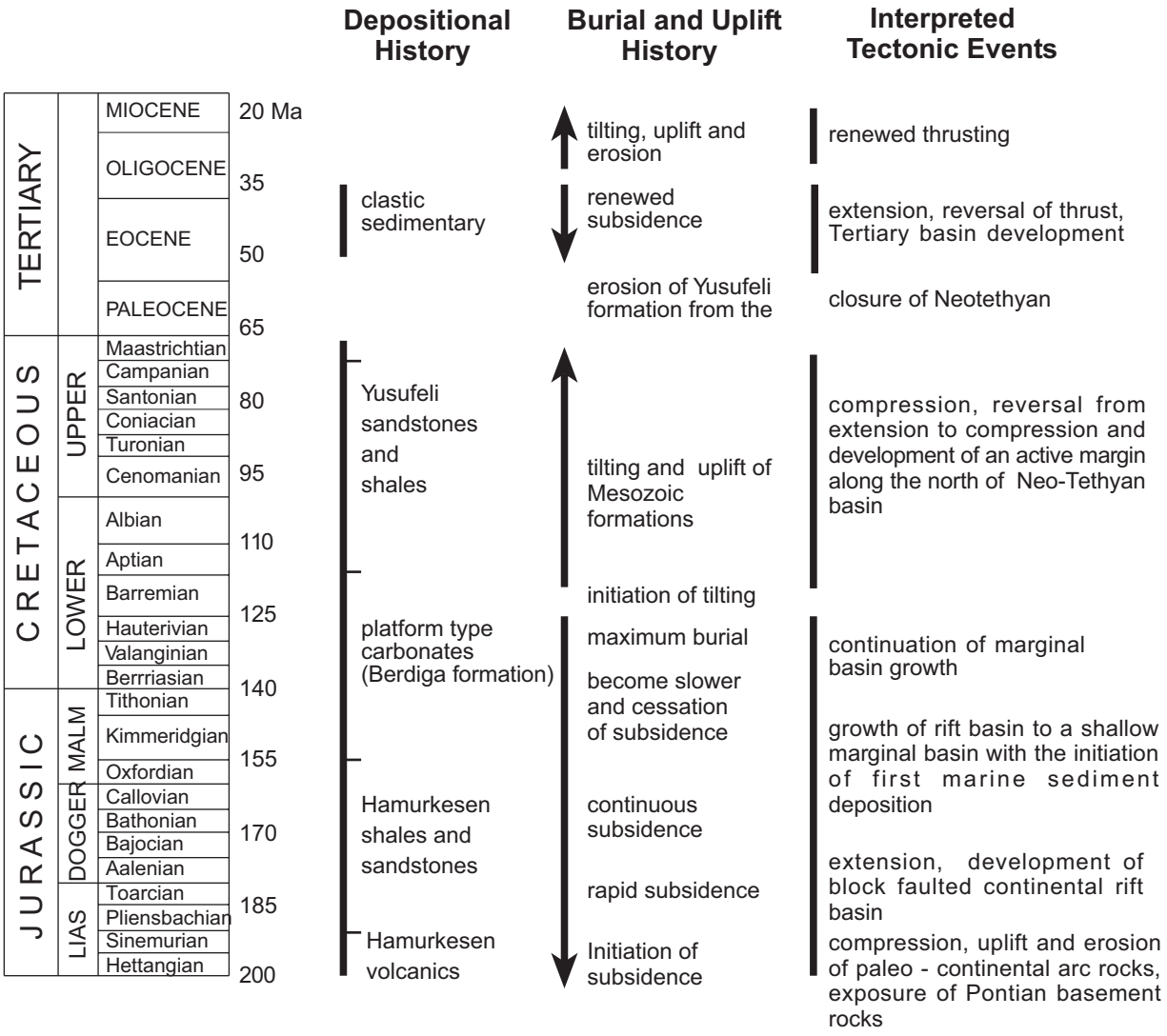

Figure 13. Summary and chronology of events from Early Jurassic to present in the Yusufeli area, Turkey.

(Hamurkesen formation) of the Mesozoic sequence was deposited. During this stage the basin is interpreted to have been in an intra-arc or a back-arc setting with respect to the Early Jurassic Pontian arc to the north (Şengör &Yılmaz 1981; Koçyiğit *et al.* 1992; Ustaömer & Robertson 1993; Yılmaz *et al.* 1997; Okay & Şahintürk 1977). Back-arc extension in response to generation of the magmatic arc may lead to rapid subsidence and accumulation of coarse-clastic sediments in the deeper parts of the basin. In so far as the basin was tectonically unstable during this period, the horst sites – especially those near the shore of the basin – could not have received clastic sediments and may have remained as source areas to grabens even though they were below sea level. The absence of carbonates in the Lower Jurassic profiles probably demonstrates that sedimentation was relatively rapid and that the region was near the shore to the north of the Neotethyan basin. Throughout the time in which the horst-graben topography of the basin was smoothed out, sedimentation seems to have dominated in graben sites. The variable thickness of the Lower Jurassic successions and the occurrence or absence of coarse clastics at the bottoms of the successions may be explained by this horst-graben topography of seafloor.

Then, as the basin gradually deepened with its smooth base topography and with the possible decrease in tectonic activity, it became a suitable environment for the deposition of shales, as abundantly represented in the upper parts of the Lower Jurassic successions. The existence of some basaltic sills within the formation suggests that back-arc extension in the south advanced and led to break-up in the arc to the north. Therefore, during this period, detritus may have been derived from the Late Palaeozoic arc where mainly volcanic rocks of calc-alkaline character were exposed, along with subordinate metamorphic rocks and granites. There seems to have been little or no contribution of detritus originating from syn-rift volcanic rocks due to their position at the base of succession. Conformably overlying platform-type carbonates (the Berdiga formation) are the end products of this extensional regime, and were deposited from the Kimmeridgian to the Cenomanian; these are characterized by thin-bedded micritic limestone at the base, but acquire a thick or massive bedded structure upwards. Thus, the basin may be interpreted to have formed during a period in which subsidence relatively slowed or ceased, even though upper parts of it may have been compressed or uplifted in the Aptian or Albian.

The third stage of the basin coincided with deposition of Yusufeli formation, which generally comprises turbidites. Upward coarsening in clast size and bed thickness in the unit indicates that the basin was filled gradually. A likely tectonic scenario may have involved a reverse in tectonic style from extension to compression and development of an active margin along the northern side of the Neotethyan basin (Şengör & Yımaz 1981; Koçyiğit 1991; Tüysüz *et al.* 1995; Yılmaz *et al.* 1997; Okay & Şahintürk 1997). Red clastics, up to 23 m thick at the base of Ormandibi profile, were the first deposits of the Yusufeli formation over the carbonate rocks and tend to show higher CIA indices in compared to the grey to green clastics of the unit. All of these data suggest that a long, tectonically stable period and oxidizing climatic conditions in the source area(s) prevailed during the deposition of carbonates from the Kimmeridgian to the Barremian. Additionally, a sudden transition from deposition of carbonates to red clastics in the Aptian may be interpreted as a transition from a tectonically stable situation to an unstable one, and as initiation of uplift in the source area. Consequently, there was a change in the weathering conditions of the source area(s), such as from intensely oxidizing weathering to predominantly physical weathering. The other red horizons in the upper levels of the unit may also be interpreted as products of crustal provenance areas, where arid climatic conditions and static periods (in terms of crustal movements) prevailed during particular periods prior to intense physical weathering and transportation. Until the end of the Palaeocene, the present-day Yusufeli area was above sea level (Robinson *et al.* 1995; Okay *et al.* 2001). Thus, nearly all of the Upper Cretaceous formations were eroded from atop the eastern Pontides.

The other short-lived change in tectonic regime – from compression to extension – occurred in the mid-Eocene. After a short period of extension, which is known as the Lutetian transgression throughout the Pontides (Şengör & Yılmaz 1981; Okay *et al.* 1997, 2001; Yılmaz *et al.* 1997), this area and the whole Pontian belt were affected by renewed compression and, hence, a final episode of tilting, uplift and erosion occurred.

Conclusions

In the present study, standard petrographic techniques were combined with major- and trace element analyses in order to elucidate the provenance, sedimentary history and geochemistry of the Lower Jurassic and Upper Cretaceous terrigenous rocks of the Yusufeli area (Artvin, Turkey). Petrographic and geochemical data indicate that the sediment source for Lower Jurassic and Upper Cretaceous rocks can be directly related to moderately evolved volcanic-arc rocks. Thus, the likely source terrain seems to have comprised pre-Jurassic volcanic rocks, and very possibly the volcanic rocks of a Late Palaeozoic Pontian arc which are presently not exposed (or no longer exist). La/Sc, Th/Sc, Cr/Th, Co/Th and Cr/Ni ratios, which are good indicators of provenance, demonstrate that at least two types of rocks were exposed in the source area and provided detritus to the basin, consisting of a dominant mafic volcanic source and a subordinate felsic volcanic source.

Mineral fractionation is not observed in the rocks, indicating compound influences on REE distribution rather than a single, selective one. However, positive correlation between Zr and LREEs and between HREEs and Y and P_2O_5 in the Upper Cretaceous samples indicates that zircon, hornblende and phosphate minerals seem to have at least partially controlled REE distribution.

High SiO_2 contents and the LREE-depleted patterns of the shales relative to associated sandstones in the PAAS-normalised plot indicate enrichment in silt-sized quartz particles, which have a low total REE content even though they yield an LREE-enriched pattern. This situation may be regarded as an effect of hydraulic sorting on REE chemistry.

The average CIA indices for subaerial weathering indicate that the source terrain for the Lower Jurassic and Upper Cretaceous sediments was not affected by intense chemical weathering. However, a distinct upward (stratigraphically) increase in shale/sand ratio and CIA indices in the Lower Jurassic profile suggest that the source area underwent gradually intensifying chemical weathering, possibly due to a decrease in tectonic activity. In contrast, a general upward decrease in CIA indices in the Upper Cretaceous profiles demonstrates that the sediments were derived from a gradually less-weathered source terrain, reflecting increased erosion rates likely due to increasing tectonic activity. However, red horizons in the unit may correspond to periods in which tectonic activity and erosion slowed and weathering increased.

Acknowledgements

The authors thank Kemal Erdoğan (General Directorate of Mineral Research and Exploration [MTA], Ankara) for his determination of fossil assemblages from our thin sections. The manuscript was constructively reviewed by A. Sami Derman, N. Terzioğlu and an anonymous referee; their insightful comments are gratefully acknowledged.

References

Adamia, S.A., Lordkipanidze, M.B. & Zakariadze, G.S. 1977. Evolution of an active continental margin as exemplified by the Alpine history of the Caucasus. *Tectonophysics* **40**, 183–199

Akin, H. 1978. Geologie, Magmatismus und Lagerstaettenbildung im ostpontischen Gebirge-Turkei aus der Sicht der plattentektonik. *Geologische Rundschau* **68**, 253–283.

Akinci, Ö.T. 1984. The eastern Pontide volcano-sedimentary belt and associated massive sulphide deposits. *In*: Dixon, J.E. & Robertson A.H.F. (eds), *The Geological Evolution of the Eastern Mediterranean*. Geological Society, London Special Publications **17**, 415–428.

Alp, D. 1972. *Amasya Yöresinin Jeolojisi [Geology of Amasya Region]*. Ph.D. İstanbul Üniversitesi Fen Fakültesi Monografileri Tabii İlimler Kısmı **22**, 101 p.

Aslan, Z. 2005. Petrography and petrology of the calc-alkaline Sarıhan granitoid (NE Turkey): an axample of magma mingling and mixing. *Turkish Journal of Earth Sciences* **14**, 183–207.

Arslan, M., Tüysüz, N., Korkmaz, S. & Kurt, H. 1997. Geochemistry and petrogenesis of the eastern Pontide volcanic rocks, Northeast Turkey. *Chemie der Erde* **57**, 157–187.

Banfield, J.F. & Eggelton, R.A. 1989. Apatite replacement and rare earth mobilization, fractionation and fixation during weathering. *Clays and Clay Minerals* **37**, 113–127.

Bektaş, O., Pelin, S. & Korkmaz, S. 1984. Doğu Pontid yay gerisi havzasında manto yükselimi ve polijenik ofiyolit olgusu [The rise of mantle in the eastern Pontide back-arc basin and polygenic ophiolite fact]. *Türkiye Jeoloji Kurumu Ketin Sempozyumu*, 175–188 [in Turkish with English abstract].

Bektaş, O., Şen, C., Atici, Y. & Köprübaşı, N. 1999. Migration of the Upper Cretaceous subduction-related volcanism towards the back arc basin of the eastern Pontide magmatic arc (NE Turkey). *Geological Journal* **34**, 95–106.

Bergougnan, H. 1987. *Etudes geologiques dans l'Est Anatolien*. PhD Thesis, University Pierre et Marie Curie, France, 606 p.

Bhatia, M.R. & Crook, K.A.W. 1986. Trace element characteristics of graywackes and tectonic setting Discrimination Of Sedimentary Basin. *Contributions To Mineralogy And Petrology* **92**, 181–193.

Bozkurt, E. & Mittwede, S.K. 2001. Introduction to the geology of Turkey–a synthesis. *International Geology Review* **43**, 578–594.

Bozkuş, C. 1990. *Olur-Kömürlü-Akşar (Erzurum) Arasının Stratigrafik ve Tektonik Özellikleri [Stratigraphic and Tectonic Characteristics of Olur-Kömürlü-Akşar (Erzurum) Area]*. PhD Thesis, Cumhuriyet Üniversitesi, Sivas, Türkiye, 162 p [in Turkish with English abstract, unpublished].

Chatalov, A.G. 1991. Triassic in Bulgaria. *In*: Dewey, J.F. (ed), *Special Issue on Tectonics*. Bulletin of the Technical University of İstanbul **44**, 103–135.

Condie, K.C. 1993. Geochemical composition and evolution of the upper continental crust: contrasting results from surface samples and shales. *Chemical Geology* **104**, 1–37.

Condie, K.C., Dengate, J. & Cullers, R.L. 1995. Behavior of rare earth elements in a paleoweathering profile on granodiorite in the front range, Colorado, USA. *Geochimica et Cosmochimica Acta* **59**, 279–294.

Condie, K.C. & Wronkijewicz, D.J. 1990. The Cr/Th ratio in Precambrian pelites from the Kaapvaal craton as an index of craton evolution. *Earth and Planetary Science Letters* **97**, 256–267.

Creaser, R.A., Erdmer, P., Stevens, R.A. & Grant, S.L. 1997. Tectonic affinity of Nisutlin and Avil assemblages strata from the Teslin tectonic zone, northern Canadian Cordillera: constraints from neodymium isotope and geochemical evidence. *Tectonics* **16**, 107–121.

CULLERS, R.L. 1994. The controls on the major and trace element variation of shales, siltstones, and sandstones of Pennsylvanian-Permian age from uplifted continental blocks in Colorado to platform sediment in Kansas, USA. *Geochimica et Cosmochimica Acta* **58**, 4955–4972.

CULLERS, R.L., BARRET, T., CARLSON, R. & ROBINSON, B. 1987. Rare earth element and mineralogical changes in Holocene soil and stream sediment: a case study in the Wet Mountains, Colorado, USA. *Chemical Geology* **63**, 275–295.

Cullers, R.L., Basu, A. & Suttner, L. 1988. Geochemical signature of provenance in sand-size material in soils and stream sediments near the Tobacco Root batholith, Montana, USA. Chemical Geology 70, 335–348.

CULLERS, R.L., CHAUDHURI, S., KILBANE, N. & KOCH, R. 1979. Rare earths in size fractions and sedimentary rocks of Pennsylvanian-Permian age from the mid-continent of the USA. *Geochimica et Cosmochimica Acta* **43**, 1285–1301.

ÇOĞULU, E. 1975. *Gümüşhane ve Rize Granitik Plütonlarının Mukayeseli Petrojeolojik ve Jeokronometrik Etüdü [Petrologic and Geochronological Investigation and Comparison of Gümüşhane and Rize Plutons]*. DSc Thesis, İstanbul Technical University Publications **1034**, İstanbul, 112 p [in Turkish with English abstract, unpublished].

DES MARAIS D.J. 1994. The Archean atmosphere: its composition and fate. *In*: CONDIE, K.C. (ed), *Archean Crustal Evolution*. Developments in Precambrian Geology **11**, Elsevier.

DEAN, W.T. 2005. Trilobites from the Çal Tepe formation (Cambrian), near Seydişehir, central Taurides, southwestern Turkey. *Turkish Journal of Earth Sciences* **14**, 1–71.

DICKINSON, W.R., BEARD, L.S., BRAKENRIDGE, G.R., ERJAVEC, J.L., FERGUSON, R.C., INMAN, K.F., KNEPP, R.A., LINDBERG, F.A. & RYBERG, P.T. 1983. Provenance of North American Phanerozoic sandstone in relation to tectonic setting. *Geological Society of America Bulletin* **93**, 222–235.

DICKINSON, W.R. & SUCZEK, C.A. 1979. Plate tectonics and sandstone compositions. *American Association of Petroleum Geologists Bulletin* **63**, 2164–2182.

DOKUZ, A. 2000. *Yusufeli (Artvin-Türkiye) Yöresinin Jeolojisi, Jeotektoniği, Magmatik-Metamorfik Kayaçların Jeokimyası ve Petrojenezi [Geology, Geotectonics, Geochemistry and Petrogenesis of Magmatic and Metamorphic Rocks in Yusufeli (Artvin-Turkey)]*. PhD Thesis, Karadeniz Teknik Üniversitesi, Trabzon, Türkiye, 311 p [in Turkish with English abstract, unpublished].

DOTT, R.H. 1964. Wacke, graywacke and matrix: what approach to immature sandstone classification? *Journal of Sedimentary Petrology* **34**, 625–632.

ERDOĞAN, B. & GÜNGÖR, T. 2004. The problem of the core-cover boundary of the Menderes Massif and an emplacement mechanism for regionally extensive gneissic granites, western Anatolia (Turkey). *Turkish Journal of Earth Sciences* **13**, 15–36.

FEDO, C.M., ERIKSSON, K.A. & KROGSTAD, E.J. 1996. Geochemistry of shales from the Archean (~ 3.0 Ga) Buhwa Greenstone Belt, Zimbabwe: implications for provenance and source area weathering. *Geochimica et Cosmochimica Acta* **60**, 1751–1763.

FLOYD, P.A., ÖZGÜL, M. & GÖNCÜOĞLU, C. 2003. Metabasite blocks from the Koçkaya HP-LT metamorphic rocks, Konya, central Anatolia: geochemical evidence for an arc-back-arc pair? *Turkish Journal of Earth Sciences* **12**, 157–174.

GEDİKOĞLU, A., PELİN, S. & ÖZSAYAR, T. 1979. The main lines of geotectonic development of the east Pontides in the Mesozoic era: *Proceedings of the 1st Geological Congress of the Middle East* (GEOCOME), 555–580.

GERDJIKOV, I. 2005. Alpine metamorphism and granitoid magmatism in the Strandja zone: new data from the Sakar unit, SE Bulgaria. *Turkish Journal of Earth Sciences* **14**, 167–183.

GÖTZE, J. 1998. Geochemistry and provenance of the Altendorf feldspathic sandstone in the Middle Bunter of the Thuringian basin, Germany. *Chemical Geology* **150**, 43–61.

GRANDSTAFF, D.E., EDELMAN, M.J., FOSTER, R.W., ZBINDEN, E. & KIMBERLEY, M.M. 1986. Chemistry and mineralogy of Precambrian paleosols at the base of the Dominion and Pongola groups (Transvaal, South Africa). *Precamrian Research* **32**, 97–131.

KARSLI, O., AYDIN, F. & SADIKLAR, M.B. 2004. Magma interaction recorded in plagioclase zoning in granitoid systems, Zigana granitoid, Eastern Pontides, Turkey. *Turkish Journal of Earth Sciences* **13**, 287–305.

KASTING, J.F. 1993. Earth's early atmosphere. *Science* **259**, 920–926

KESKİN, İ., KORKMAZ, S., GEDİK, İ., ATEŞ, M., GÖK, L., KÜÇÜMEN, Ö. & ERKAL, T. 1989. *Geology of the Region Around Bayburt.* Maden Tetkik ve Arama Genel Müdürlüğü (MTA), Report No. 8995, 128 p [in Turkish, unpublished].

KIMBERLEY, M.M. & HOLLAND, H.D. 1992. Introduction to Precambrian weathering and paleosols. *In*: SCHIDLOWSKI, M., GOLUBIC, S., KIMBERLEY, M.M., MCKIRDY, D.M. & TRUDINGER, P.A. (eds), *Early Organic Evolution:. Implications for Mineral and Energy Resources*, Springer, 9–15.

KETIN, İ. 1966. Tectonic units of Anatolia (Asia Minor). *MTA Bulletin* **66**, 23–34

KOÇYİĞİT, A. 1991. An example of an accretionary fore-arc basin from northern central Anatolia and its implications for the history of subduction of Neotethys in Turkey. *Geological Society of America Bulletin* **103**, 22–36.

KOÇYİĞİT, A., ALTINER, D., FARINACCI, A., UMBERTO, N. & CONTI M.A. 1992. Late Triassic-Aptian evolution of the Sakarya divergent margin: implications for the opening history of the northern Neotethys in northwest Anatolia, Turkey. *Geologica Romana* **27**, 81–99.

KORALAY, E., DORA, O.Ö., CHEN, F., SATIR, M. & CANDAN, O. 2004. Geochemistry and geochronology of orthogneisses in the Derbent (Alaşehir) area, eastern part of the Ödemiş-Kiraz Submassif: Pan-African magmatic activity. *Turkish Journal of Earth Sciences* **13**, 37–61.

MAYNARD, J.B., VALLONI, R. & YU, H.S. 1982. Composition of modern deep-sea sands from arc related basins. *In*: LEGGET, J.K (ed), *Trench-Forearc Geology: Sedimentation and Tectonics on Modern and Ancient Active Plate Margins*. Geological Society, London, Special Publications **10**, 551–561.

MCBRIDE, E.F. 1963. Diagenetic processes that affect provenance determinations in sandstone. *In*: ZUFFA, G.G. (ed), *Provenance of Arenites.* Reidel Dordrecht, 95–114.

MCLENNAN, S.M. 1989. Rare earth elements in sedimentary rocks: influence of provenance and sedimentary processes. *In*: LIPIN, B.R. & MCKAY, G.A. (eds), *Geochemistry and Mineralogy of REE*. Reviews in Mineralogy **21**, 169–200.

MCLENNAN, S.M., HEMMING, S.R., MCDANIEL, D.K. & HANSON, G.N. 1993. Geochemical approaches to sedimentation, provenance and tectonics. *In*: JHONSON, M.J & BASU, A. (eds), *Processes Controlling the Composition of Clastic Sediments.* Geological Society of America Special Paper **284**, 21–40.

MCLENNAN, S.M., TAYLOR, S.R. & KRONER, A. 1983. Geochemical evolution of Archean shales from South Africa: I. the Swaziland and Pongola Supergroups. *Precambrian Research* **22**, 93–124.

MCLENNAN, S.M., TAYLOR, S.R., MCCULLOCH, M.T. & MAYNARD, J.B. 1990. Geochemical and Nd-Sr isotopic composition of deep-sea turbidites: crustal evolution and plate tectonic associations. *Geochimica et Cosmochimica Acta* **54**, 2015–2050.

NESBITT, H.W. 1979. Mobility and fractionation of REE during weathering of granodiorite. *Nature* **279**, 206–210.

NESBITT, H.W., MARKOVICS, G. & PRICE, R.C. 1980. Chemical processes affecting alkalis and alkaline earths during continental weathering. *Geochimica et Cosmochimica Acta* **44**, 1659–1666.

NESBITT, H.W. & YOUNG, G.M. 1982. Early Proterozoic climate and plate motions inferred from major element chemistry of lutites. *Nature* **299**, 715–717.

NESBITT, H.W. & YOUNG, G.M. 1984. Predictions of some weathering trends of plutonic and volcanic rocks based on thermodynamic and kinetic considerations. *Geochimica et Cosmochimica Acta* **48**, 1523–1534.

NESBITT, H.W. & YOUNG, G.M. 1989. Formation and diagenesis of weathering profiles. *Journal of Geology* **97**, 129–147.

OKAY, A.İ. 1996. Granulite facies gneisses from the Pulur region, eastern Pontides. *Turkish Journal of Earth Sciences* **5**, 55–61.

OKAY, A.İ. & GÖNCÜOĞLU, C. 2004. The Karakaya complex: a review of data and concepts. *Turkish Journal of Earth Sciences* **13**, 75–95.

OKAY, A.İ. & ŞAHİNTÜRK, Ö. 1997. Geology of the eastern Pontides. *In*: ROBINSON A.G. (ed), *Regional and Petroleum Geology of the Black Sea and Surrounding Region*. AAPG Memoir **68**, 291–311.

OKAY, A.İ., TANSEL, İ. & TÜYSÜZ, O. 2001. Obduction, subduction and collision as reflected in the Upper Cretaceous–Lower Eocene sedimentary record of western Turkey. *Geological Magazine* **138**, 117–142.

ÖZER, E. 1984. The geology of Bayburt (Gümüşhane) region. *Karadeniz Teknik Üniversitesi Dergisi Jeoloji* **3**, 77–89.

PETTIJOHN, F.J., POTTER, P.E. & SIEVER, R. 1987. *Sand and Sandstone* (2nd ed). Springer, Berlin, Heidelberg, NewYork.

PICKETT, E.A. & ROBERTSON, A.H.F. 2004. Significance of the volcanogenic Nilüfer unit and related components of the Triassic Karakaya Complex for Tethyan subduction/accretion. *Turkish Journal of Earth Sciences* **13**, 97–143.

REIMER, T.O. 1985. Volcanic rocks and weathering in the Early Proterozoic Witwatersrand Supergroup, South Africa. *Geololgical Survey of Finland Bulletin* **331**, 33–49.

ROBINSON, A.G., BANKS, C.J., RUTHERFORD, M.M. & HIRST, J.P.P. 1995. Stratigraphic and structural development of the eastern Pontides, Turkey. *Journal of the Geological Society, London* **152**, 861–872.

ROSER, B.P. & KORSCH, R.J. 1985. Plate tectonics and geochemical composition of sandstones: a discussion. *Journal of Geology* **93**, 81–84.

ROSER, B.P. & KORSCH, R.J. 1986. Determination of tectonic setting of sandstone-mudstone suites using SiO_2 content and K_2O/Na_2O ratio. *Journal of Geology* **94**, 635–694.

SLACK, J.F. & STEVENS, P.J. 1994. Clastic metasediments of the Early Proterozoic Broken Hill Group, New South Wales, Australia: geochemistry, provenance, and metallogenic significance. *Geochimica et Cosmochimica Acta* **58**, 3633–3652.

ŞEN, C., ARSLAN, M. & VAN, A. 1998. Geochemical and petrological characteristics of eastern Pontide Eocene (?) alkaline volcanic province, NE Turkey. *Turkish Journal of Earth Sciences* **7**, 231–239.

ŞENGÖR, A.M.C. & YILMAZ, Y. 1981. Tethyan evolution of Turkey: a plate tectonic approach. *Tectonophysics* **75**, 181–241.

ŞENGÖR, A.M.C., YILMAZ, Y. & KETİN, İ. 1980. Remnants of Pre-Late Jurassic ocean in northern Turkey: fragments of Permian-Triassic Paleo-Tethys. *Geological Society of America Bulletin* **91**, 599–609.

SPADEA, P., TORTORICI, L. & LANZAFAME, G. 1980. Ophiolites of Tyrrhenian coastal chain. *In*: BORTOLOTTI, V. (ed), *VIth Ophiolite Field Conference, Field Excursion Guidebook.* Gruppo Lavoro Ofioliti Mediterranee, Florence, Italy, 19–27.

TAYLOR, S.R. & MCLENNAN, S.M. 1985. *The Continental Crust: Its Composition and Evolution.* Oxford, Blackwell Scientific Publishing, 312 p.

TOKEL, S. 1977. Doğu Karadeniz bölgesinde Eosen yaşlı kalk-alkalen andezitler ve jeeotektonizma [Geotectonics and Eocene calc-alkaline andesites in eastern Black Sea region]. *Türkiye Jeoloji Kurumu Bülteni* **20**, 49–54 [in Turkish with English abstract].

TOPUZ, G. & ALTHERR, R. 2004. Pervasive rehydration of granulites during exhumation – an example from the Pulur complex , eastern Pontides, Turkey. *Mineralogy and Petrology* **81**, 165–185.

TOPUZ, G., ALTHERR, R., KALT, A., SATIR, M., WERNER, O. &. SCHWARZ, W.H. 2004. Aluminous granulites from the Pulur complex, NE Turkey: a case of partial melting, efficient melt exctraction and crystallisation. *Lithos* **72**, 183–207.

TÜYSÜZ, O. 1990. Tectonic evolution of a part of the Tethyside orogenic collage: the Kargı Massif, northern Turkey. *Tectonics* **9**, 141–160.

TÜYSÜZ, O., DELLALOĞLU, A.A. & TERZİOĞLU, N. 1995. A magmatic belt within the Neo-Tethyan suture zone and its role in the tectonic evolution of northern Turkey. *Tectonophysics* **243**, 173–191.

USTAÖMER, T. & ROBERTSON, A.H.F. 1993. A Late Palaeozoic-Early Mesozoic marginal basin along the active southern continental margin of Eurasia: evidence from the central Pontides (Turkey) and adjacent regions. *Geological Journal* **28**, 219–238.

WRONKIJEWICZ, D.J & CONDIE, K.C. 1987. Geochemistry of Archean shales from the Witwatersand supergroup, South Africa: source area weatheing and provenance. *Geochimica et Cosmochimica Acta* **51**, 2401–2416.

WRONKIJEWICZ, D.J & CONDIE, K.C. 1989. Geochemistry and provenance of sediments from the Pongola Supergroup, South Africa: evidence for a 3.0 Ga-old continental craton. *Geochimica et Cosmochimica Acta* **53**, 1537–1549.

WRONKIJEWICZ, D.J & CONDIE, K.C. 1990. Geochemistry and mineralogy of sediments from the Ventersdrop and Transvaal supergroups, South Africa: cratonic evolution during the Early Proterozoic. *Geochimica et Cosmochimica Acta* **54**, 343–354.

YILMAZ, Y. 1972. *Petrology and Structure of the Gümüşhane Granite and Surrounding Rocks, North-Eastern Anatolia.* PhD Thesis, University of London, 260 p [unpublished].

YILMAZ, Y., TÜYSÜZ, O., YİĞİTBAŞ, E., GENÇ, Ş.C. & ŞENGÖR, A.M.C. 1997. Geology and tectonic evolution of the Pontides. *In*: ROBINSON, A.G. (ed), *Regional and Petroleum Geology of the Black Sea and Surrounding Region*. AAPG Memoir **68**,183–226.

YILMAZ, A. & YILMAZ, H. 2004. Geology and structural evolution of the Tokat Massif, eastern Pontides, Turkey. *Turkish Journal of Earth Sciences* **13**, 231–246.

YOUNG, G.M. 1991. The geologic record of glaciation: relevance to the climatic history of the earth. *Geoscience Canada* **18**, 100–108.

Received 02 February 2005; revised typescript accepted 25 November 2005